Effect of Segregation on the Course of Unpremixed Polymerizations

Reactant segregation and mixing effects can be represented by a one-dimensional distribution of alternating reactive liquid layers. This paper reports a theoretical study of the influence of this configuration on the course of three-component, random block copolymerizations. Two models that follow the interdiffusion of the reacting species and the catalyst are considered. The first employs a lumped competitive-parallel kinetic scheme to represent the formation of hard and soft segments; the second uses a moment formulation to handle the polymerization. The results are intended for the description of mixing-activated three-component polyurethane systems, but conclusions of a general nature are obtained. Several unexpected results are presented regarding the molecular weight buildup and spatial product segregation in the system. In particular, it is established that reactant segregation may severely influence product segregation (layering), the average molecular weight, and the maximum molecular weight achieved.

S. D. Fields, J. M. Ottino
Departments of Chemical Engineering and
Polymer Science and Engineering
University of Massachusetts
Amherst, MA 01003

Introduction

To date, mixing effects of polymerizations, particularly diffusional effects, have received little attention in the literature. Most works have focused on gross analysis based on classical reaction engineering using a macromixing-micromixing approach. However, this viewpoint is not appropriate for unpremixed polymerizations; in these cases it is imperative to account for diffusional effects. With processes such as polymerizations in extruders (Chella and Ottino, 1982) or static mixers (Ottino and Chella, 1983) and reaction injection molding (RIM) (Chella and Ottino, 1983) becoming more important commercially, a fundamental understanding of the influence of coupled mixing-diffusional effects is required for predicting the influence of mixing on polymer properties. In this paper we single out RIM as a prototype for understanding micromixing effects for unpremixed polymerizations. It is the unpremixed polymerization about which the most is known, and since the fluid-mechanical mixing is relatively fast, only diffusional effects need be considered.

Several investigators (Lee et al., 1980; Kolodziej et al., 1982) have demonstrated that the mixing step is the key to producing good RIM materials. This is because the RIM process requires that two reactive monomer phases be intimately mixed in a very short period of time; sometimes this results in imperfect mixing. It has been conjectured by Lee, Kolodziej, and their respective coworkers that RIM impingement mixing produces alternating striations of the monomer phases, and thus the polymerization occurs at a set of interfaces.

A surprisingly small number of attempts have been made toward modeling a polymerization at an interface. Sokolov and Nikonov gave a qualitative description of interfacial polymerizations in Millick and Carraher (1977), whereas Ranz (1979) and Lee et al. (1980) presented a very simplified diffusion-controlled pseudosteady-state model for the RIM polymerization at an interface. Kolodziej et al. (1982) used a qualitative interfacial model to explain possible product segregation for the case of three-component polyurethane polymerizations. To date, the only model to contain enough complexity to describe an imperfectly mixed RIM interfacial polymerization is the work by Chella and Ottino (1983). These authors modeled a two-component, catalyzed crosslinking polyurethane interfacial polymerization by means of a set of partial differential equations for the diffusion-reaction process and included concentration-dependent diffusivities. Their main assumptions were:

1. The reaction is lumped and second order, i.e., the reaction was $A^e + B^e \rightarrow P$, where A^e and B^e are monomer endgroups and P is the polymer.

2. The catalyst, which is initially mixed with A, diffuses quickly achieving uniform concentration in short time scales.

The current address of S. D. Fields is Rohm and Haas Company, Bristol, PA 19007.
Correspondence concerning this paper should be addressed to J. M. Ottino

3. The interfacial zone is stable.
4. The system is locally adiabatic.

Chella and Ottino used this model to explain the experimental results of Lee et al.; an incomplete reaction (asymptotic conversion less than unity) could occur even with stoichiometric reactants. According to the model this was due to the shutdown of the polymerization when an impermeable polymer region formed in the neighborhood of the interface. It showed also that an increase in catalyst concentration (intrinsic rate of reaction) or initial temperature gave decreased asymptotic conversion. This was again due to an impervious polymer region that formed near the interface; higher initial reaction rates tended to build up sharper regions, causing monomer segregation and decreased conversion. However, two major questions remain:

- How does domain formation and product distribution occur in linear phase separating polymerizations?
- How does imperfect mixing affect the molecular weight distribution of the polymer formed?

Both questions have implications on morphological studies (Chen et al., 1983), since the spatial distribution of hard and soft domains and the molecular weight distribution dictate many of the final properties of the polymeric sample.

The basic building block for an unpremixed polymerization is a single interface or an elementary pair of striations. Two models are presented here to simulate diffusion and reaction for step growth polymerizations at this length scale. The physical situation corresponds to the case in which mechanical mixing is achieved in short time scales.

In this paper we use a lamellar mixing model to describe an imperfectly mixed, fast, three-component, random block copolymerization. In the most general case, a polymerization occurring in a reactor with concurrent fluid-mechanical mixing, the results presented here can be considered to apply to a microflow element; for details, see Chella and Ottino (1984) and Fields (1985). Extensions of the current work to include striation thickness distribution and fluid mechanical history effects are considered elsewhere (Fields and Ottino, 1987a,b). The objective here is to provide information about how reactant (monomer) segregation influences the nature of the polymer produced; only results that display interesting qualitative features will be presented. The analysis is broken into two parts. In the first section a lumped competitive-parallel kinetic scheme is used to study product segregation. In the second section a moment formulation is employed to obtain molecular weight information.

Reacting System

Physical situation

We consider one-dimensional striations with a monodisperse striation thickness distribution for each monomer phase. (The region in the neighborhood of the interface between the monomer phases is, in general, much more complicated than this: Fields et al. [1986]; however, one-dimensional segregation is a good starting point for understanding the important effects.) We solve the mass and energy balances over a region from the centerline of a polyol striation to the centerline of the neighboring diisocyanate striation. The underlying assumptions governing the physical situation are detailed below and are similar to those of Chella and Ottino (1983). The differences are that a mobile catalyst is contained in the diol phase, and a different model is adopted for the diffusion coefficients.

Assumptions

The relevant assumptions are:

1. The monomers and polymer are stagnant. All species have the same density.

2. The segregation is represented by monodisperse striations, Figure 1. The initial concentrations for the diol phase are (dimensionless concentrations):

$$C_i = 1 \quad \text{for} \quad 0 < x < s_A \quad \text{and} \quad C_i = 0 \quad \text{for} \quad s_A < x < 1$$

Likewise, the initial concentrations for the diisocyanate phase are:

$$C_i = 0 \quad \text{for} \quad 0 < x < s_A \quad \text{and} \quad C_i = 1 \quad \text{for} \quad s_A < x < 1$$

3. The no-flux boundary conditions at the centerlines of the striations are:

$$\frac{\partial C_i}{\partial x} = 0 \quad \text{at} \quad x = 0, 1$$

4. Assuming no convection and Fickian diffusion, without cross-diffusion terms, the dimensionless mass balances are:

$$\frac{\partial C_i}{\partial t} = \Delta_i \left[\frac{\partial}{\partial x} \left(D_i \frac{\partial C_i}{\partial x} \right) \right] + D_{am} \xi_i r_i$$

5. The temperature rise is uniform and the system is locally adiabatic (Chella and Ottino, 1983). Thus, the energy balance reduces to:

$$\frac{dT}{dt} = \gamma \frac{d\bar{C}_B}{dt}$$

This is a particularly good assumption for polymeric systems since the thermal diffusivity is much greater than the mass diffusivities.

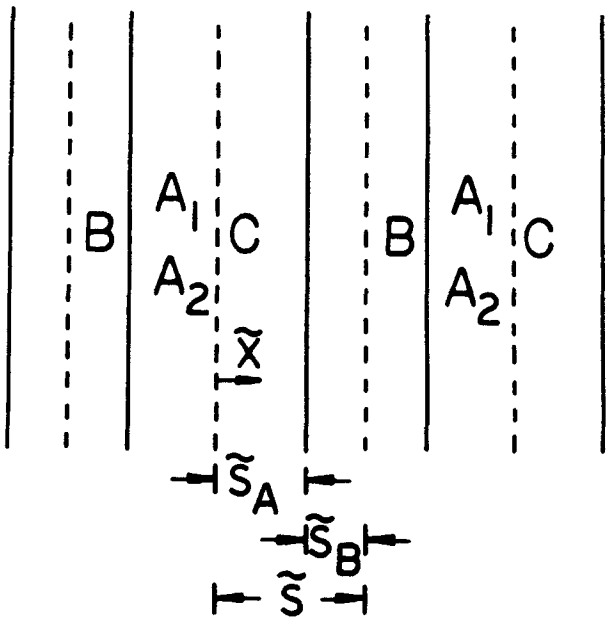

Figure 1. Monodisperse striations.

6. The diffusion coefficients are a function of the local composition, for the monomers (reactants) and the polymer products do not diffuse. The diffusion coefficient functionality adopted here is based on the Stokes-Einstein equation (Bird et al., 1960), that is, inversely proportional to both the size of the diffusing species and the viscosity of the medium. A model for the viscosity of the medium is based on the old model by Kendall and Monroe (1917), but any other appropriate expression could be adopted without changing the qualitative character of the results. These are combined to obtain the following model for the dimensionless effective diffusivity of species i:

$$D_i = D_i^T(\tilde{T})D_i^C(\tilde{C})$$

where

$$D_i^T(\tilde{T}) = \exp(-E_i^d/R\tilde{T})/\exp(-E_i^d/R\tilde{T}^0)$$

$$D_i^C(\tilde{C}) = \tilde{\mu}_B\left(\sum_j \tilde{C}_j\right)^3 \Big/ \left(\sum_j (\tilde{C}_j)(\tilde{\mu}_j)^{1/3}\right)^3$$

$\tilde{\mu}_B$ = reference viscosity

$\tilde{\mu}_j$ = viscosity of component j

In this model the concentration-dependent part of the dimensionless diffusivity is the same for all species since it is only a function of the local composition. If all the diffusion activation energies are assumed to be equal, then the temperature-dependent part of the dimensionless diffusivities is also the same for all species. This model predicts a slower decrease of the mobility of species with increasing polymer concentration in comparison with the percolation behavior adopted by Chella and Ottino (1983), which is more suited for crosslinking systems.

Parameters

The system of equations detailed above is a set of coupled partial differential equations for the mass balances and several algebraic equations for the energy balance and the diffusivities. There are many parameters in this set of equations, and some cannot be estimated by independent experiments at the moment. The monomer concentrations, densities, viscosities, and molecular weights were estimated by consulting the literature and manufacturers' specifications for RIM urethane monomers. The heat capacity, heat of reaction, and rate expressions were taken from work by Richter and Macosko (1978). (The rate constant given by Richter and Macosko was adjusted to give realistic times of reaction under unpremixed conditions.) The diffusion coefficients were estimated from literature values for the diffusion of small molecules in viscous liquids (Cussler, 1984). The activation energies for diffusion were taken from the computations of Chella and Ottino (1983). The remaining parameters, which may be chosen arbitrarily, represent the initial conditions (stoichiometry, initial temperature, initial catalyst concentration) and the mixing level (striation thickness).

Numerical method

The method of lines (MOL) was chosen because it works well for solving stiff partial differential equations. In this method, the spatial domain is discretized at a number of nodes and the diffusion terms in the mass balances are approximated using centered finite differences. The resulting set of coupled ordinary differential equations (ODE) was solved using the GEARB package (Hindmarsh, 1977). Typically, 50 to 200 nodes were found sufficient to give good accuracy. If steep gradients existed early in the simulation, the nodes were concentrated in a region near the initial interface.

Lumped Competitive-Parallel Model

As a simple representation of the three-component, random block copolymerization, one may use a lumped competitive parallel kinetic scheme:

$$A_1^e + B^e \xrightarrow{C} P_1$$

$$A_2^e + B^e \xrightarrow{C} P_2$$

where:

A_1^e = short diol endgroup

A_2^e = long diol endgroup

B^e = diisocyanate endgroup

C = catalyst

P_1 = hard segment

P_2 = soft segment

In this formulation, A_1 and A_2 monomers are diols and B is a diisocyanate. When either an A_1 or an A_2 endgroup reacts with a B endgroup a urethane linkage is formed. Obviously, other chemical interpretations are possible. The reaction between an A_1 molecule and a B molecule produces a so-called hard segment, P_1, and the reaction between an A_2 molecule and a B molecule produces a so-called soft segment, P_2. There is no calculation of molecular weight in this model.

The results of Richter and Macosko (1978) are used to model the kinetics:

$$\tilde{r}_{A_1}^e = -k_1(\tilde{C}_{A_1}^e)(\tilde{C}_B^e)(\tilde{C}_C)^{3/4}\exp(-E_1/R\tilde{T})$$

$$\tilde{r}_{A_2}^e = -k_2(\tilde{C}_{A_2}^e)(\tilde{C}_B^e)(\tilde{C}_C)^{3/4}\exp(-E_2/R\tilde{T})$$

Thus,

$$r_{A_1}^e = -(C_{A_1}^e)(C_B^e)(C_C)^{3/4}\exp\left[-\frac{E_1}{R}\left(\frac{1}{\tilde{T}} - \frac{1}{\tilde{T}^0}\right)\right]$$

$$r_{A_2}^e = -\frac{\tilde{C}_{A_2}^0}{\tilde{C}_{A_1}^0}(C_{A_2}^e)(C_B^e)(C_C)^{3/4}\exp\left[-\frac{1}{R}\left(\frac{E_2}{\tilde{T}} - \frac{E_1}{\tilde{T}^0}\right)\right]$$

$$r_B^e = r_{A_1}^e + r_{A_2}^e$$

$$r_C = 0$$

$$r_{P_1} = -r_{A_1}^e$$

$$r_{P_2} = -r_{A_2}^e$$

The numerical simulation described above was solved with several choices for the parameters. The base case parameters are listed in Table 1. Again, the parameter values were chosen to approximate an actual RIM system without making any attempt at curve fitting.

Table 1. Base Case Parameters for Lumped Competitive-Parallel Model

$\tilde{C}^{e^0}_{A_1} = 3.55\ \text{kmol/m}^3$	$\tilde{T}^0 = 298\ \text{K}$
$\tilde{C}^{e^0}_{A_2} = 8.87 \times 10^{-1}\ \text{kmol/m}^3$	Molar ratio: 5/4/1 ($B/A_1/A_2$)
$\tilde{C}^{e^0}_{B} = 8.66\ \text{kmol/m}^3$	$\rho_{A_1} = 1{,}017.1\ \text{kg/m}^3$
$\tilde{C}^{0}_{C} = 5.0 \times 10^{-4}\ \text{kmol/m}^3$	$\rho_{A_2} = 1{,}053\ \text{kg/m}^3$
$\tilde{s} = 1.0 \times 10^{-4}\ \text{m}$	$\rho_{B} = 1{,}244\ \text{kg/m}^3$
$s_A = 0.66$	$\rho_{P_1} = 1{,}122\ \text{kg/m}^3$
$s_B = 0.34$	$\rho_{P_2} = 1{,}122\ \text{kg/m}^3$
$\tilde{D}^{e^0}_{A_1} = 1.0 \times 10^{-10}\ \text{m}^2\text{/s}$	$MW_{A_1} = 90.12\ \text{kg/kmol}$
$\tilde{D}^{e^0}_{A_2}/\tilde{D}^{e^0}_{A_1} = 0.04506$	$MW_{A_2} = 2{,}000.0\ \text{kg/kmol}$
$\tilde{D}^{e^0}_{B}/\tilde{D}^{e^0}_{A_1} = 0.679$	$MW_{B} = 287.4\ \text{kg/kmol}$
$\tilde{D}^{0}_{C}/\tilde{D}^{e^0}_{A_1} = 0.2613$	$MW_{P_1} = 377.52\ \text{kg/kmol}$
$E^d_{A_1} = E^d_{A_2} = E^d_B = E^d_C = 4.184 \times 10^4\ \text{kJ/kmol}$	$MW_{P_2} = 2{,}287.4\ \text{kg/kmol}$
$k_1 = k_2 = 1.4 \times 10^8\ \text{m}^{21/4}/\text{kmol}^{7/4} \cdot \text{s}$	$\tilde{\mu}_{A_1} = 7.46 \times 10^{-2}\ \text{Pa} \cdot \text{s}$
$E_1 = E_2 = 4.41 \times 10^4\ \text{kJ/kmol}$	$\tilde{\mu}_{A_2} = 8.424 \times 10^{-1}\ \text{Pa} \cdot \text{s}$
$C_p = 2.2\ \text{kJ/kg} \cdot \text{K}$	$\tilde{\mu}_{B} = 3.0 \times 10^{-2}\ \text{Pa} \cdot \text{s}$
$\Delta H_R = -1.03 \times 10^5\ \text{kJ/(kmol NCO)}$	$\tilde{\mu}_{P_1} = 10.0\ \text{Pa} \cdot \text{s}$
$R = 8.31\ \text{kJ/kmol} \cdot \text{K}$	$\tilde{\mu}_{P_2} = 1.0\ \text{Pa} \cdot \text{s}$

The results may be displayed in the form of concentration profiles for both the reactants and the products. For a moderate time ($\tilde{t}$ = 50 s) in the base case polymerization, the concentration profiles across the striation are shown in Figure 2. Our primary interest focuses on the possibility of phase segregation due to diffusion limitations.

Figure 2a displays the interdiffusion of the monomers and the subsequent overlap of the monomer concentration profiles. The concentration gradient of the long diol is larger than that of the short diol due to the smaller diffusivity of the long diol. This favors production of hard segment material, especially on the diisocyanate side of the interface, when compared to the production of soft segment material, Figure 2b. Note that relatively little soft segment is produced on the diisocyanate side of the interface. Both polymer concentration profiles show maxima on the diol side of the interface since the catalyst is initially contained there. Figure 3 displays the same information at a later time ($\tilde{t}$ = 150 s). Most of the monomers have been consumed and the catalyst is almost uniform at this point in the polymerization, Figure 3a. A large fraction of the long diol remains unreacted at this time, whereas nearly all of the short diol has been consumed; this is a direct consequence of their relative mobilities. The polymer product concentrations have grown, but the same qualitative behavior remains, Figure 3b.

Figures 2b and 3b indicate that the polymer products may be segregated due to diffusion-reaction interactions. This is more evident in Figure 4a, where the hard and soft segment volume fractions are plotted vs. position. Hard segment volume fraction is defined here as the volume of the hard segment divided by the total volume of the polymer: $\phi_{P_1} = \tilde{V}_{P_1}/(\tilde{V}_{P_1} + \tilde{V}_{P_2})$. An analogous definition is used for the soft segment. There is a region on the diisocyanate side of the interface that is predominately hard segment. This observation gives strength to the arguments given by Chang et al. (1982), Chen et al. (1983), and Kolodziej et al. (1982) to explain the morphology of polyurethanes. Thus, the appearance of hard segment-rich globules noted by Chang et al. in their morphological studies may be the result of imperfect mixing.

Since the diffusion coefficients are functions of concentration, their values vary across the striation. This is shown in Figure 4b,

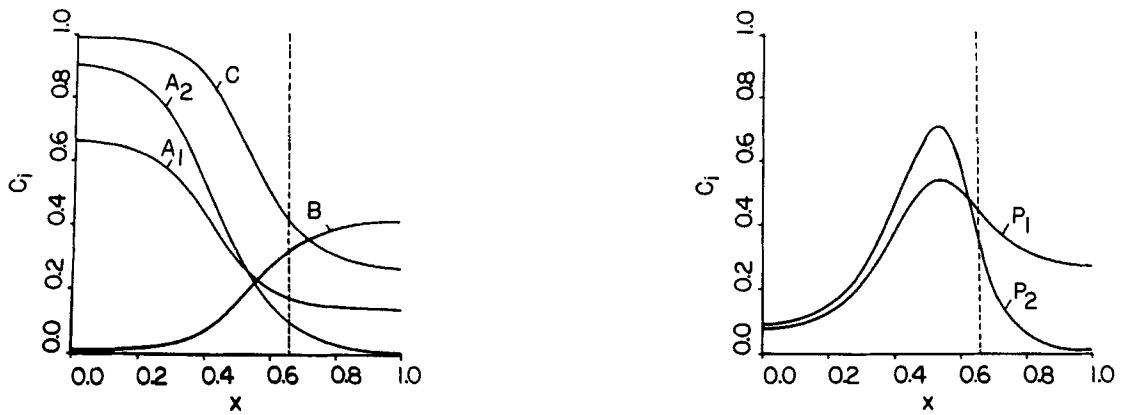

Figure 2. Competitive-parallel model, $\tilde{t}$ = 50 s, base case parameters.

a. Monomer and catalyst concentration profiles

b. Polymer product concentration profiles

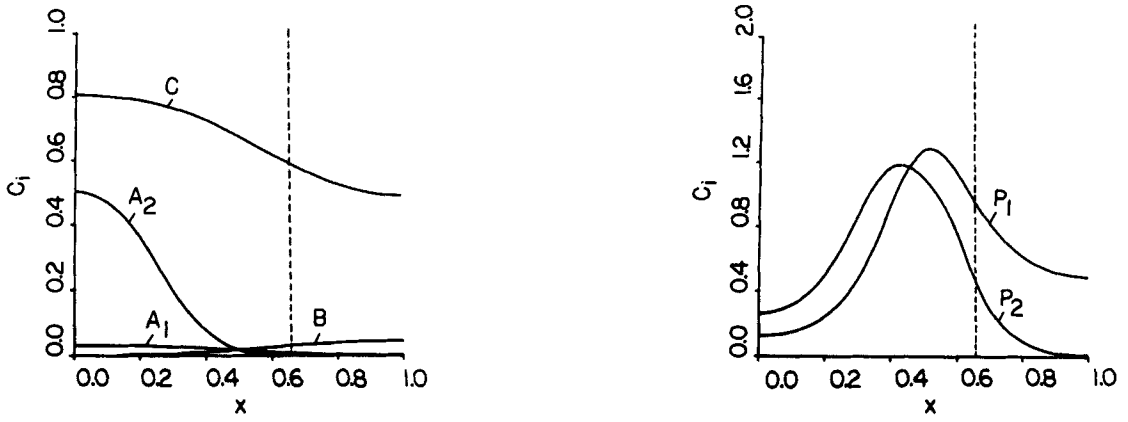

Figure 3. Competitive-parallel model, $\tilde{t}$ = 150 s, base case parameters.

a. Monomer and catalyst concentration profiles

b. Polymer product concentration profiles

in which the dimensionless diffusivity, D_i, is plotted vs. dimensionless distance. D_i has a minimum that corresponds to the maxima in the polymer concentration profiles. The local polymer concentration, especially the hard segment concentration, is the controlling factor for the local diffusion coefficients.

Mixing level effects

This model is very mixing-sensitive. Runs were made varying the striation thickness while holding all other parameters constant. The range of mixing levels explored includes striation thicknesses five times smaller than the base case (base case $\tilde{s}$ = 0.01 cm) to five times larger than the base case. This corresponds to a Damköhler number range of 3.0×10^{-1} to 1.9×10^{2}.

The most obvious consequence noted when the mixing level (striation thickness) is varied is the length of time required to achieve nearly complete conversion of the monomers. Since the reactions under consideration are irreversible and stoichiometric, the long time behavior is full conversion of the monomers. Nevertheless, a polymer region is formed in the neighborhood of the original interface which hinders monomer interdiffusion. This phenomenon can limit conversion to values significantly below unity for reasonable times under poorly mixed conditions ($\tilde{s}$ > 0.01 cm). A more detailed analysis of this phenomenon is given later.

Monomer concentration profiles

The mixing level affects the monomer and catalyst concentration profiles in two ways. As the mixing level is increased, the monomer and catalyst concentration profiles become flatter, and the amount of unreacted monomers remaining at a given time decreases. This may be seen by comparing Figure 2a (base case) to Figure 5a for a striation thickness five times smaller than the base case, and to Figure 5b for a striation thickness five times larger than the base case.

Polymer concentration and volume fraction profiles

The mixing level strongly affects the polymer concentration profiles, as may be seen by comparing Figure 2b (base case) to Figure 6a (base case $\tilde{s}$ decreased 5×) and Figure 6b (base case $\tilde{s}$ increased 5×). Under better mixing conditions, Figure 6a, the polymer concentration profiles are flatter, and the segregation of hard and soft segments is reduced. This plot shows a hard segment concentration profile that is nearly uniform and a soft segment profile that is only moderately segregated. In contrast, under poor mixing conditions, Figure 6b, the polymer product

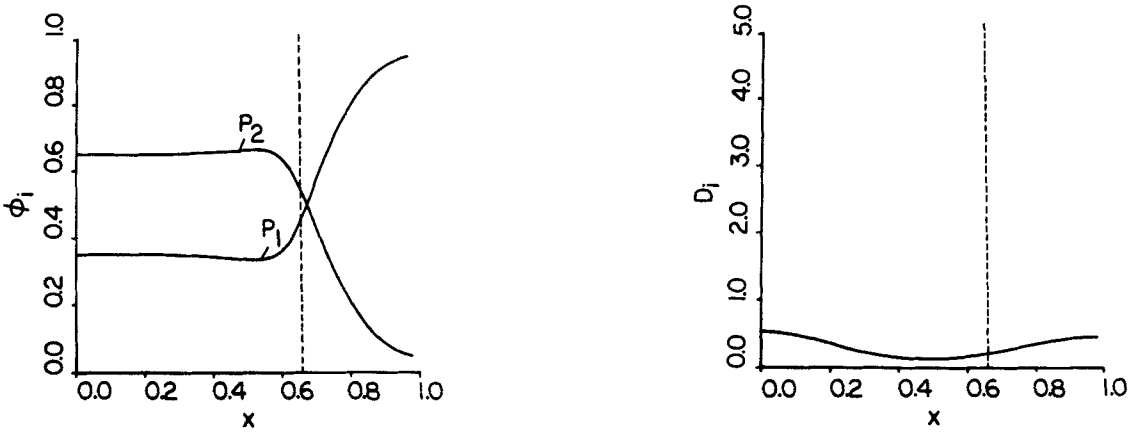

Figure 4. Competitive-parallel model, $\tilde{t}$ = 50 s, base case parameters.

a. Polymer volume fraction profiles

b. Diffusion coefficient profile

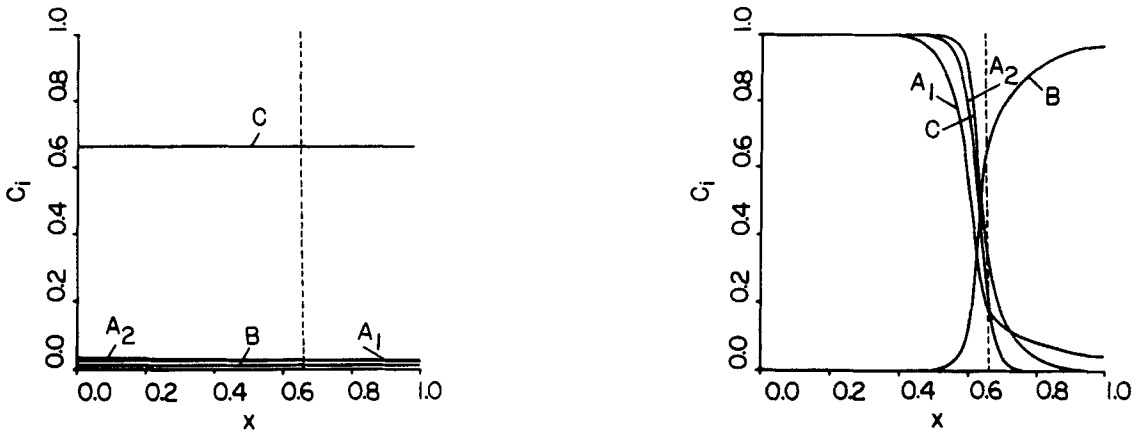

Figure 5. Competitive-parallel model, $\tilde{t}$ = 50 s, monomer and catalyst concentration profiles.

a. Striation thickness decreased 5×

b. Striation thickness increased 5×

profiles form much sharper peaks than were seen in the base case. The products are more effectively segregated on the diisocyanate side of the interface than was seen under better mixing conditions. This is due to the small penetration distance of the long diol (A_2) into the diisocyanate.

The long-time behavior of the simulation for poor mixing conditions gives somewhat unexpected behavior. An inflection develops in the soft segment (P_2) profile, as shown in Figure 7a. (Also shown in the polymer volume fraction profiles in Figure 7b.) This is manifested by the local region of monomer concentration profile overlap shifting toward the diol striation at long times. This results from the formation of the polymer layer in the neighborhood of the interface, which decreases the diffusion of the diols and the catalyst into the diisocyanate phase more than it decreases the diffusion of the diisocyanate into the diol phase. This effect is more severe for the long diol (A_2) and produces a more noticeable shift in the location of the soft segment formation than that for the hard segment. The soft segment profile may be thought of as a sum of several peaks with a significant displacement between them, resulting in the inflection. Although the hard segment is also the sum of several peaks, the shift between them is smaller, resulting in a single peak with no inflection. This phenomenon is not seen for the base case, but is noticeable for striation thicknesses of 0.02 and 0.05 cm. The effect is more pronounced as the mixing level is decreased.

Lumped model summary

The lumped model does not provide any information about the nature of the polymer formed in a mixing-activated urethane polymerization. It is natural that in addition to the concentration of polymer formed, one would like to know the concentration of polymer endgroups (zero moments) across the striation, the average and spatial distribution of the molecular weight, and ideally, the polydispersity and sequence length distribution of the polymer. A second polymerization model was developed which incorporates zero and first moment equations for a three-component, random block copolymerization.

Moment Formulation Model

In this formulation, A_1 and A_2 monomers are diols and B is a diisocyanate. When either an A_1 or an A_2 endgroup reacts with a B endgroup a urethane linkage is formed. As in the lumped formulation, the reaction between an A_1 molecule and a B molecule produces a hard segment, and the reaction between an A_2 molecule and a B molecule produces a soft segment. The polymer formed from this random block copolymerization is of the type

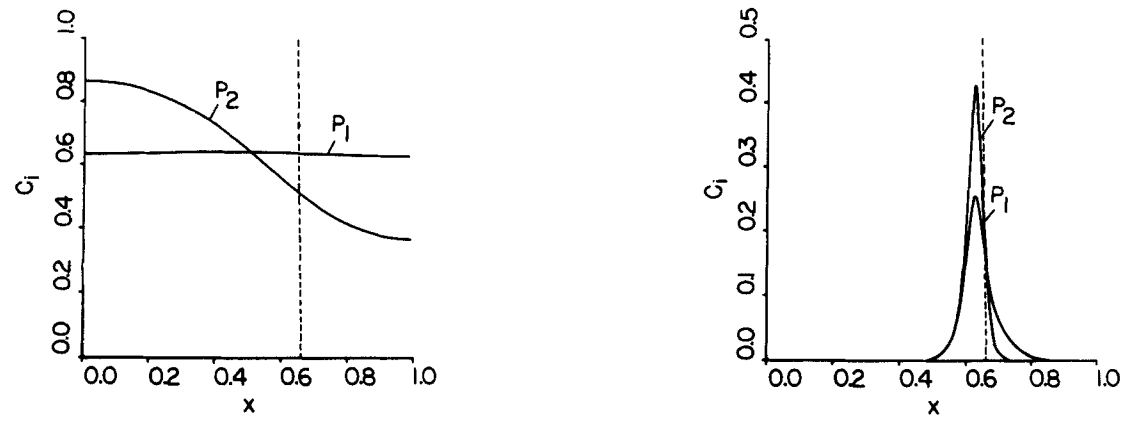

Figure 6. Competitive-parallel model, $\tilde{t}$ = 50 s, polymer product concentration profiles.

a. Striation thickness decreased 5×

b. Striation thickness increased 5×

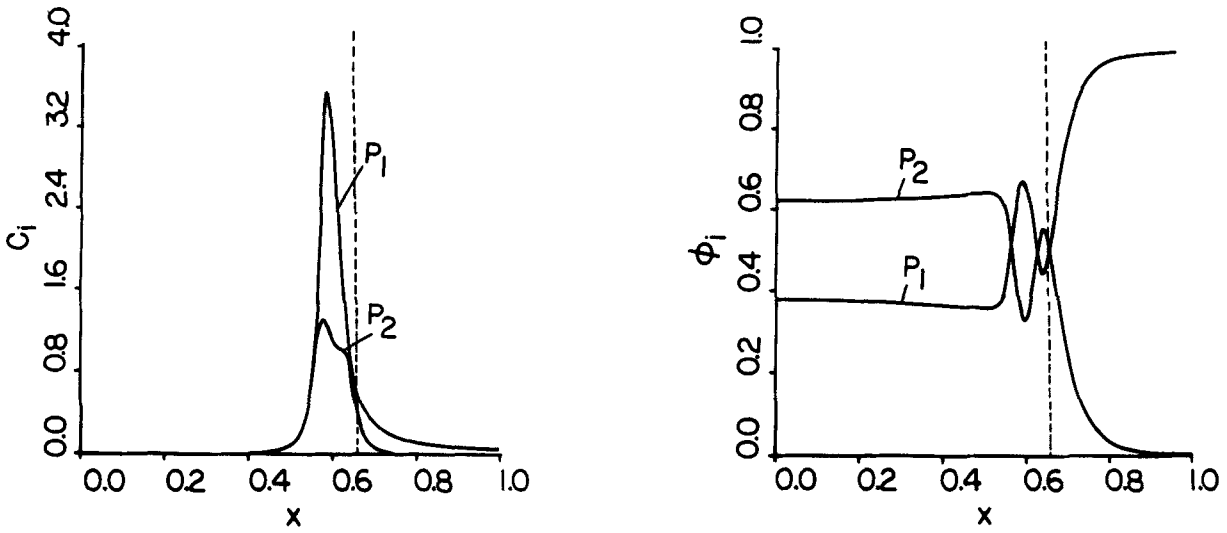

Figure 7. Competitive-parallel model, $\tilde{t}$ = 1,250 s, striation thickness increased 5×.

a. Polymer product concentration profiles

b. Polymer volume fraction profiles

. . . *ABABABABAB* . . . with each *A* representing either an A_1 or an A_2 monomer. Double moments are required due to the incorporation of both type A_1 and type A_2 monomers into the polymer chains. To ease the formulation, only three populations of polymer molecules are differentiated from each other, those with two *A*-type ends (either A_1 or A_2), those with one *A*-type end and one *B*-type end, and those with two *B* ends. It is assumed that A_1 and A_2 ends are equally reactive with *B* ends so that it is not important to keep track of which type *A* monomer is on the end of a given polymer chain. Also, only the composition of the polymer species is followed; sequence information is not incorporated into this model.

Thus, let $AA_{n,m}$ represent the concentration of polymer molecules with two *A* endgroups containing *n* A_1 molecules and *m* A_2 molecules. Since *A* and *B* must alternate, there are $(n + m - 1)$ *B* molecules in such a polymer chain. A similar definition is used for $AB_{n,m}$ (one *A* and one *B* endgroup) and $BB_{n,m}$ (two *B* endgroups). In the model that follows, each reaction of the type:

$$\text{=}A + \text{—}B \xrightarrow{C} \text{=}AB\text{—}$$

is assumed to occur with the same kinetic expression:

$$\tilde{r}^e_A = \tilde{r}^e_B = -k''(\tilde{C}^e_A)(\tilde{C}^e_B)(\tilde{C}_C)^{c^*} \exp(-E/R\tilde{T}) \quad (1)$$

That is, the rate of consumption of a particular polymer species is a function only of its endgroup types and concentrations. Each kinetic expression is first order in both *A* and *B* endgroup concentrations and is c^*th order in catalyst concentration. In Eq. 1 $\tilde{r}^e_i$ is the rate of production of endgroup type *i* and $\tilde{C}^e_i$ is the concentration of endgroup type *i*. The possible reactions for this system are detailed in Table 2. They are standard condensation reactions for a random block copolymerization and follow directly from the polymer species definitions and the resulting possible combinations of monomer and polymer types. These reactions and the kinetic expression in Eq. 1 yield the reaction source terms in Table 3.

Moment method

Since we desire to compute the zero and first moments for each polymer species, we define the moments (exemplified for $AB_{n,m}$) as:

$$\tilde{\alpha}\tilde{\beta}_{kl} = \sum_{n=0}^{\infty}\sum_{m=0}^{\infty} n^k m^l \tilde{C}_{AB_{n,m}}$$

The moments $\tilde{\alpha}\tilde{\alpha}_{kl}$ for $AA_{n,m}$ and $\tilde{\beta}\tilde{\beta}_{kl}$ for $BB_{n,m}$ are defined in an analogous manner.

One may also define the following generating functions (Tirrell et al. 1987):

$$AA(s_1, s_2) = \sum_{n=0}^{\infty}\sum_{m=0}^{\infty} s_1^n s_2^m \tilde{C}_{AA_{n,m}}$$

$$AB(s_1, s_2) = \sum_{n=0}^{\infty}\sum_{m=0}^{\infty} s_1^n s_2^m \tilde{C}_{AB_{n,m}}$$

$$BB(s_1, s_2) = \sum_{n=0}^{\infty}\sum_{m=0}^{\infty} s_1^n s_2^m \tilde{C}_{BB_{n,m}}$$

where s_1 and s_2 are dummy variables. The differential equations

Table 2. Random Block Copolymerization Reactions

$A_1 + B \rightarrow AB_{1,0}$
$A_2 + B \rightarrow AB_{0,1}$
$AA_{n,m} + B \rightarrow AB_{n,m}$
$AA_{n,m} + AB_{i,j} \rightarrow AA_{n+i,m+j}$
$AA_{n,m} + BB_{i,j} \rightarrow AB_{n+i,m+j}$
$AB_{n,m} + A_1 \rightarrow AA_{n+1,m}$
$AB_{n,m} + A_2 \rightarrow AA_{n,m+1}$
$AB_{n,m} + B \rightarrow BB_{n,m}$
$AB_{n,m} + AB_{i,j} \rightarrow AB_{n+i,m+j}$
$AB_{n,m} + BB_{i,j} \rightarrow BB_{n+i,m+j}$
$BB_{n,m} + A_1 \rightarrow AB_{n+1,m}$
$BB_{n,m} + A_2 \rightarrow AB_{n,m+1}$

Table 3. Kinetic Source Terms for a Three-Component, Random Block Copolymerization

$$\tilde{r}_{A_1} = -2k\tilde{C}_{A_1}\tilde{C}_B\tilde{C}_C^{c*} - k\tilde{C}_{A_1}\sum_{n=0}^{\infty}\sum_{m=0}^{\infty}\tilde{C}_{AB_{n,m}}\tilde{C}_C^{c*} - 2k\tilde{C}_{A_1}\sum_{n=0}^{\infty}\sum_{m=0}^{\infty}\tilde{C}_{BB_{n,m}}\tilde{C}_C^{c*}$$

$$\tilde{r}_{A_2} = -2k\tilde{C}_{A_2}\tilde{C}_B\tilde{C}_C^{c*} - k\tilde{C}_{A_2}\sum_{n=0}^{\infty}\sum_{m=0}^{\infty}\tilde{C}_{AB_{n,m}}\tilde{C}_C^{c*} - 2k\tilde{C}_{A_2}\sum_{n=0}^{\infty}\sum_{m=0}^{\infty}\tilde{C}_{BB_{n,m}}\tilde{C}_C^{c*}$$

$$\tilde{r}_B = -2k\tilde{C}_{A_1}\tilde{C}_B\tilde{C}_C^{c*} - 2k\tilde{C}_{A_2}\tilde{C}_B\tilde{C}_C^{c*} - 2k\tilde{C}_B\sum_{n=0}^{\infty}\sum_{m=0}^{\infty}\tilde{C}_{AA_{n,m}}\tilde{C}_C^{c*} - k\tilde{C}_B\sum_{n=0}^{\infty}\sum_{m=0}^{\infty}\tilde{C}_{AB_{n,m}}\tilde{C}_C^{c*}$$

$$\tilde{r}_{AA_{n,m}} = -2k\tilde{C}_B\tilde{C}_{AA_{n,m}}\tilde{C}_C^{c*} - k\tilde{C}_{AA_{n,m}}\sum_{i=0}^{\infty}\sum_{j=0}^{\infty}\tilde{C}_{AB_{i,j}}\tilde{C}_C^{c*} + k\sum_{i=0}^{n-1}\sum_{j=0}^{m-1}\tilde{C}_{AA_{n-i,m-j}}\tilde{C}_{AB_{i,j}}\tilde{C}_C^{c*} - 2k\tilde{C}_{AA_{n,m}}\sum_{i=0}^{\infty}\sum_{j=0}^{\infty}\tilde{C}_{BB_{i,j}}\tilde{C}_C^{c*}$$
$$+ k\tilde{C}_{A_1}\tilde{C}_{AB_{n-1,m}}\tilde{C}_C^{c*} + k\tilde{C}_{A_2}\tilde{C}_{AB_{n,m-1}}\tilde{C}_C^{c*}$$

$$\tilde{r}_{AB_{n,m}} = 2k\tilde{C}_{AA_{n,m}}\tilde{C}_B\tilde{C}_C^{c*} - k\tilde{C}_{AB_{n,m}}\sum_{i=0}^{\infty}\sum_{j=0}^{\infty}\tilde{C}_{AA_{i,j}}\tilde{C}_C^{c*} + 2k\sum_{i=0}^{n-1}\sum_{j=0}^{m-1}\tilde{C}_{AA_{n-i,m-j}}\tilde{C}_{BB_{i,j}}\tilde{C}_C^{c*} - k\tilde{C}_{A_1}\tilde{C}_{AB_{n,m}}\tilde{C}_C^{c*} - k\tilde{C}_{A_2}\tilde{C}_{AB_{n,m}}\tilde{C}_C^{c*} - k\tilde{C}_B\tilde{C}_{AB_{n,m}}\tilde{C}_C^{c*}$$
$$- k\tilde{C}_{AB_{n,m}}\sum_{i=0}^{\infty}\sum_{j=0}^{\infty}\tilde{C}_{AB_{i,j}}\tilde{C}_C^{c*} + \left(\frac{1}{2}\right)k\sum_{i=0}^{n-1}\sum_{j=0}^{m-1}\tilde{C}_{AB_{n-i,m-j}}\tilde{C}_{AB_{i,j}}\tilde{C}_C^{c*} - k\tilde{C}_{AB_{n,m}}\sum_{i=0}^{\infty}\sum_{j=0}^{\infty}\tilde{C}_{BB_{i,j}}\tilde{C}_C^{c*}$$
$$+ 2k\tilde{C}_{A_1}\tilde{C}_{BB_{n-1,m}}\tilde{C}_C^{c*} + 2k\tilde{C}_{A_2}\tilde{C}_{BB_{n,m-1}}\tilde{C}_C^{c*} + 2k\tilde{C}_{A_1}\tilde{C}_B\delta(n-1)\delta(m)\tilde{C}_C^{c*} + 2k\tilde{C}_{A_2}\tilde{C}_B\delta(n)\delta(m-1)\tilde{C}_C^{c*}$$

$$\tilde{r}_{BB_{n,m}} = -2k\tilde{C}_{BB_{n,m}}\sum_{i=0}^{\infty}\sum_{j=0}^{\infty}\tilde{C}_{AA_{i,j}}\tilde{C}_C^{c*} + k\tilde{C}_B\tilde{C}_{AB_{n,m}}\tilde{C}_C^{c*} - k\tilde{C}_{BB_{n,m}}\sum_{i=0}^{\infty}\sum_{j=0}^{\infty}\tilde{C}_{AB_{i,j}}\tilde{C}_C^{c*} + k\sum_{i=0}^{n-1}\sum_{j=0}^{m-1}\tilde{C}_{BB_{n-i,m-j}}\tilde{C}_{AB_{i,j}}\tilde{C}_C^{c*}$$
$$- 2k\tilde{C}_{A_1}\tilde{C}_{BB_{n,m}}\tilde{C}_C^{c*} - 2k\tilde{C}_{A_2}\tilde{C}_{BB_{n,m}}\tilde{C}_C^{c*}$$

given in Table 3 may then be transformed using the generating function definitions and the moments may be obtained in the standard manner from the transformed equations. Even though the procedure is relatively straightforward, the general method is not presented in the literature, and thus the details are given in the Appendix. The resulting zero and first-order moment equations, along with the monomer balances, are given in Table 4.

The moment equations are substituted into the species diffusion equations as the reaction source terms r_i. All other assumptions from the lumped model are employed for the moment formulation. The base case parameters are listed in Table 5.

The polymerization model gives the same qualitative behavior as the lumped competitive-parallel model presented previously for the monomer, catalyst, and polymer product profiles and for the polymer volume fraction profiles. The minor differences between the results are due to the basic assumptions regarding the mobility of the reactive endgroups. In the lumped competitive-parallel model, all reactive endgroups are mobile throughout the simulation. In contrast, it is possible for the endgroups to become trapped in the polymerization model; this occurs for all endgroups attached to polymer chains. Late in the polymerization nearly all endgroups are immobile in the polymerization model, while none are in the competitive-parallel model. This results in the polymerization model being even more sensitive to mixing effects than the competitive-parallel model.

A comparison between the monomer concentration profiles shows that the polymerization model yields sharper profiles than the competitive-parallel model. This conclusion also holds for

Table 4. Dimensionless Reaction Source Terms for Polymerization Model

$$r_{A_1}^{\square} = -2\beta_1 C_{A_1} C_B C_C^{c*} - \beta_2 C_{A_1}\alpha\beta_{00} C_C^{c*} - 2\beta_2 C_{A_1}\beta\beta_{00} C_C^{c*}$$

$$r_{A_2}^{\square} = -2\beta_1 C_{A_2} C_B C_C^{c*} - \beta_2 C_{A_2}\alpha\beta_{00} C_C^{c*} - 2\beta_2 C_{A_2}\beta\beta_{00} C_C^{c*}$$

$$r_B^{\square} = -2\beta_3 C_{A_1} C_B C_C^{c*} - 2\beta_4 C_{A_2} C_B C_C^{c*} - 2\beta_2 C_B\alpha\alpha_{00} C_C^{c*} - \beta_2 C_B\alpha\beta_{00} C_C^{c*}$$

$$r_{\alpha\alpha_{00}}^{\square} = -2\beta_1 C_B\alpha\alpha_{00} C_C^{c*} - 2\beta_2\alpha\alpha_{00}\beta\beta_{00} C_C^{c*} + \beta_3 C_{A_1}\alpha\beta_{00} C_C^{c*} + \beta_4 C_{A_2}\alpha\beta_{00} C_C^{c*}$$

$$r_{\alpha\alpha_{10}}^{\square} = -2\beta_1 C_B\alpha\alpha_{10} C_C^{c*} + \beta_2\alpha\alpha_{00}\alpha\beta_{10} C_C^{c*} - 2\beta_2\alpha\alpha_{10}\beta\beta_{00} C_C^{c*} + \beta_2 C_{A_1}\alpha\beta_{00} C_C^{c*} + \beta_3 C_{A_1}\alpha\beta_{10} C_C^{c*} + \beta_4 C_{A_2}\alpha\beta_{10} C_C^{c*}$$

$$r_{\alpha\alpha_{01}}^{\square} = -2\beta_1 C_B\alpha\alpha_{01} C_C^{c*} + \beta_2\alpha\alpha_{00}\alpha\beta_{01} C_C^{c*} - 2\beta_2\alpha\alpha_{01}\beta\beta_{00} C_C^{c*} + \beta_3 C_{A_1}\alpha\beta_{01} C_C^{c*} + \beta_4 C_{A_2}\alpha\beta_{01} C_C^{c*} + \beta_2 C_{A_2}\alpha\beta_{00} C_C^{c*}$$

$$r_{\alpha\beta_{00}}^{\square} = 2\beta_1\alpha\alpha_{00} C_B C_C^{c*} - \beta_2\alpha\beta_{00}\alpha\alpha_{00} C_C^{c*} + 2\beta_2\alpha\alpha_{00}\beta\beta_{00} C_C^{c*} - \beta_3 C_{A_1}\alpha\beta_{00} C_C^{c*} - \beta_4 C_{A_2}\alpha\beta_{00} C_C^{c*} - \beta_1 C_B\alpha\beta_{00} C_C^{c*}$$
$$-\tfrac{1}{2}\beta_2\alpha\beta_{00}\alpha\beta_{00} C_C^{c*} - \beta_2\alpha\beta_{00}\beta\beta_{00} C_C^{c*} + 2\beta_3 C_{A_1}\beta\beta_{00} C_C^{c*} + 2\beta_4 C_{A_2}\beta\beta_{00} C_C^{c*} + 2\beta_5 C_{A_1} C_B C_C^{c*} + 2\beta_6 C_{A_2} C_B C_C^{c*}$$

$$r_{\alpha\beta_{10}}^{\square} = 2\beta_1\alpha\alpha_{10} C_B C_C^{c*} - \beta_2\alpha\beta_{10}\alpha\alpha_{00} C_C^{c*} + 2\beta_2\alpha\alpha_{10}\beta\beta_{00} C_C^{c*} + 2\beta_2\alpha\alpha_{00}\beta\beta_{10} C_C^{c*} - \beta_3 C_{A_1}\alpha\beta_{10} C_C^{c*} - \beta_4 C_{A_2}\alpha\beta_{10} C_C^{c*}$$
$$- \beta_1 C_B\alpha\beta_{10} C_C^{c*} - \beta_2\alpha\beta_{10}\beta\beta_{00} C_C^{c*} + 2\beta_3 C_{A_1}\beta\beta_{10} C_C^{c*} + 2\beta_2 C_{A_1}\beta\beta_{00} C_C^{c*} + 2\beta_4 C_{A_2}\beta\beta_{10} C_C^{c*} + 2\beta_1 C_{A_1} C_B C_C^{c*}$$

$$r_{\alpha\beta_{01}}^{\square} = 2\beta_1\alpha\alpha_{01} C_B C_C^{c*} - \beta_2\alpha\beta_{01}\alpha\alpha_{00} C_C^{c*} + 2\beta_2\alpha\alpha_{01}\beta\beta_{00} C_C^{c*} + 2\beta_2\alpha\alpha_{00}\beta\beta_{01} C_C^{c*} - \beta_3 C_{A_1}\alpha\beta_{01} C_C^{c*} - \beta_4 C_{A_2}\alpha\beta_{01} C_C^{c*}$$
$$-\beta_1 C_B\alpha\beta_{01} C_C^{c*} - \beta_2\alpha\beta_{01}\beta\beta_{00} C_C^{c*} + 2\beta_3 C_{A_1}\beta\beta_{01} C_C^{c*} + 2\beta_4 C_{A_2}\beta\beta_{01} C_C^{c*} + 2\beta_2 C_{A_2}\beta\beta_{00} C_C^{c*} + 2\beta_1 C_{A_2} C_B C_C^{c*}$$

$$r_{\beta\beta_{00}}^{\square} = -2\beta_2\beta\beta_{00}\alpha\alpha_{00} C_C^{c*} + \beta_1 C_B\alpha\beta_{00} C_C^{c*} - 2\beta_3 C_{A_1}\beta\beta_{00} C_C^{c*} - 2\beta_4 C_{A_2}\beta\beta_{00} C_C^{c*}$$

$$r_{\beta\beta_{10}}^{\square} = -2\beta_2\beta\beta_{10}\alpha\alpha_{00} C_C^{c*} + \beta_1 C_B\alpha\beta_{10} C_C^{c*} + \beta_2\beta\beta_{00}\alpha\beta_{10} C_C^{c*} - 2\beta_3 C_{A_1}\beta\beta_{10} C_C^{c*} - 2\beta_4 C_{A_2}\beta\beta_{10} C_C^{c*}$$

$$r_{\beta\beta_{01}}^{\square} = -2\beta_2\beta\beta_{01}\alpha\alpha_{00} C_C^{c*} + \beta_1 C_B\alpha\beta_{01} C_C^{c*} + \beta_2\beta\beta_{00}\alpha\beta_{01} C_C^{c*} - 2\beta_3 C_{A_1}\beta\beta_{01} C_C^{c*} - 2\beta_4 C_{A_2}\beta\beta_{01} C_C^{c*}$$

Table 5. Base Case Parameters for Polymerization Model

$\tilde{C}^0_{A_1} = 1.78$ kmol/m^3	$\tilde{T}^0 = 298$ K
$\tilde{C}^0_{A_2} = 4.444$ kmol/m^3	Molar ratio: 5/4/1 ($B/A_1/A_2$)
$\tilde{C}^0_B = 4.33$ kmol/m^3	
$\tilde{C}^0_C = 5.0 \times 10^{-4}$ kmol/m^3	$\rho_{A_1} = 1.0171 \times 10^3$ kg/m^3
	$\rho_{A_2} = 1.053 \times 10^3$ kg/m^3
$\tilde{s} = 1.0 \times 10^{-4}$ m	$\rho_B = 1.244 \times 10^3$ kg/m^3
$s_A = 0.66$	$\rho_{P_1} = 1.122 \times 10^3$ kg/m^3
$s_B = 0.34$	$\rho_{P_2} = 1.122 \times 10^3$ kg/m^3
$\tilde{D}^0_{A_1} = 5.0 \times 10^{-11}$ m^2/s	$MW_{A_1} = 90.23$ kg/kmol
$\tilde{D}^0_{A_2}/\tilde{D}^0_{A_1} = 0.04506$	$MW_{A_2} = 2{,}000$ kg/kmol
$\tilde{D}^0_B/\tilde{D}^0_{A_1} = 0.679$	$MW_B = 287.4$ kg/kmol
$\tilde{D}^0_C/\tilde{D}^0_{A_1} = 0.5225$	$MW_{P_1} = 377.52$ kg/kmol
	$MW_{P_2} = 2{,}287.4$ kg/kmol
$E^d_{A_1} = E^d_{A_2} = E^d_B = E^d_C = 4.184 \times 10^4$ J/mol	
$k'' = 1.4 \times 10^8$ m$^{21/4}$/kmol$^{7/4}$ · s	$\tilde{\mu}_{A_1} = 7.46 \times 10^{-2}$ Pa · s
$E = 4.41 \times 10^4$ kJ/kmol	$\tilde{\mu}_{A_2} = 8.424 \times 10^{-1}$ Pa · s
	$\tilde{\mu}_B = 3.0 \times 10^{-2}$ Pa · s
$c^* = 0.75$	$\tilde{\mu}_{P_1} = 10.0$ Pa · s
$C_p = 2.2$ kJ/kg · K	$\tilde{\mu}_{P_2} = 1.0$ Pa · s
$\Delta H_R = -1.03 \times 10^5$ kJ/kmol NCO	
$R = 8.31$ kJ/kmol · K	

the polymer product profiles and the polymer volume fraction profiles. The soft/hard/soft/hard layering is noted for smaller values of the striation thickness for the polymerization model than for the competitive-parallel model. The competitive-parallel model gives a more complete conversion in a shorter time than the polymerization model for equivalent parameters. The competitive-parallel model does predict the correct trends, though, and is a good choice for engineering calculations that do not require the additional information available from the polymerization model; it requires less than half the computer memory and execution time that the complex model does for a given set of parameters.

Zero moment profiles

Three polymer zero moment profiles at progressive times are presented in Figure 8. Note that the relative concentrations of the three polymer types are strong functions of both position and time. At short times, Figure 8a, *A–B* molecules ($\alpha\beta_{00}$) dominate due to the rapid formation of polymer molecules containing a single bond between an *A* molecule and a *B* molecule. This is especially noticeable in the neighborhood of the initial position of the interface. At this point in time there are few molecules at any location with both *A* ends or both *B* ends. At moderate times, Figure 8b, all three species are present in similar concentrations, but each polymer type has a region in which it predominates. *A–A* ($\alpha\alpha_{00}$) molecules are concentrated about the centerline of the diol phase, while *B–B* ($\beta\beta_{00}$) molecules are concentrated about the centerline of the diisocyanate phase. The *A–B* molecule concentration profile has a maximum near the initial position of the interface. At long times, Figure 8c, *A–B* molecules have essentially disappeared and molecules with both ends capped with either *A* or *B* monomers predominate. This is because *A–B* molecules can react with themselves or *A–A* or *B–B* molecules, and at long times they will disappear. Again, *A–A* molecules are concentrated about the centerline of the diol phase, while *B–B* molecules are concentrated about the centerline of the diisocyanate phase. This is a direct result of the initial location of the monomers. Polymer formed on the diol side of the

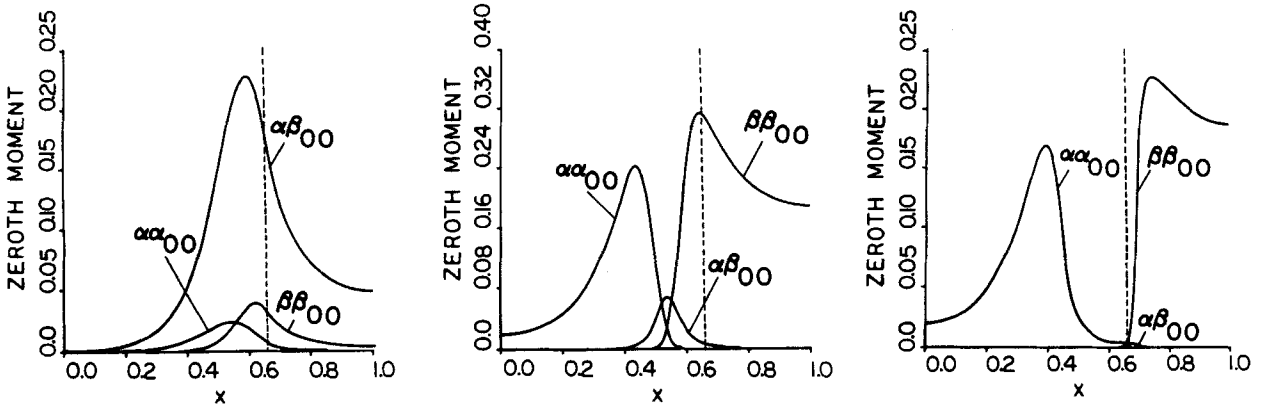

Figure 8. Zero moment profiles, base case parameters.

a. $\tilde{t} = 25$ s; b. $\tilde{t} = 150$ s; c. $\tilde{t} = 1{,}250$ s

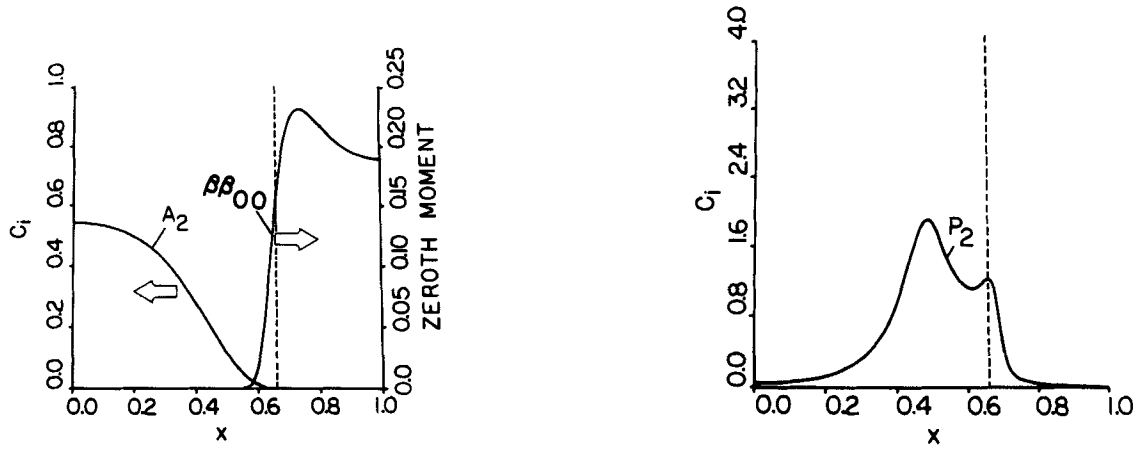

Figure 9. Formation of bimodal soft segment profile, $\bar{t}$ = 1,250 s, base case parameters.

a. Long diol and diisocyanate-endcapped polymer concentration profiles

b. Bimodal soft segment profile

interface tends to be endcapped with A molecules due to the large excess of A molecules in that region. Similar logic explains the formation of polymer molecules endcapped with B molecules on the diisocyanate side of the interface. Since the polymer molecules are not mobile in this model, the A–A and B–B molecules cannot interdiffuse, and thus the average MW levels off when only the A–A or B–B molecules are present in the system in a segregated state.

At moderate to long times, the unreacted long diol must diffuse into the diisocyanate region of the system in order to react, Figure 2a. At this point in time, there are essentially no free diisocyanate molecules; the remaining diisocyanate endgroups are segregated since they are attached to immobile polymer segments. This is demonstrated in Figure 9a, which shows the concentration profile of the long diol, A_2, plotted with the $\beta\beta_{00}$ concentration profile (zero moment for the B–B molecules). Soft segments are produced in the region of overlap of the profiles, yielding, at long times, the bimodal distribution of soft segment, shown in Figure 9b.

Degree of polymerization and molecular weight profiles

Figure 10a shows the short-time behavior of the degree of polymerization DP, which is the ratio of first to zero moments, of hard and soft segments in A–A, A–B, and B–B polymer molecules for the base case parameters. For example, $DP_{AA(A_1)}$ represents the degree of polymerization of hard segments (A_1) in A–A molecules. The DP's of the short diol are larger than those of the long diol at all positions across the striation for all polymer types. This is a result of the 4/1 (A_1/A_2) initial molar ratio chosen for the diol mixture. This plot shows that the DP profiles are relatively flat at short times. Also, the absolute values of the DP's are small, showing that only molecules up to dimers are present at this time. DP's less than one are possible due to the moment formulation.

At moderate times, Figure 10b, the DP's have a maximum on the diol side of the interface due to the catalyst initially being contained there. All three species have very similar hard segment and soft segment DP's. The system is very heterogenous, with the maximum DP being much larger than the surrounding values.

At long times, Figure 10c, the same basic structure holds for the DP profiles, but the maxima have shifted toward the diisocyanate side of the interface. This is due to the penetration of the long diol (A_2) into the (stagnant) polymer molecules. Since A_2 must react with diisocyanate endgroups, which are attached to polymer molecules on the diisocyanate side of the inferface, the

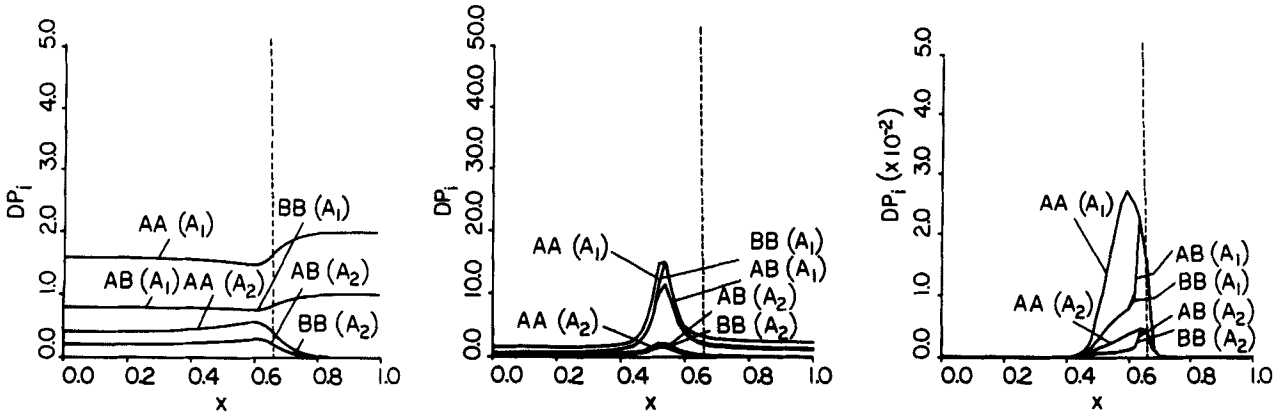

Figure 10. Degree of polymerization profiles, base case parameters.

a. $\bar{t}$ = 25 s;

b. $\bar{t}$ = 150 s;

c. $\bar{t}$ = 1,250 s

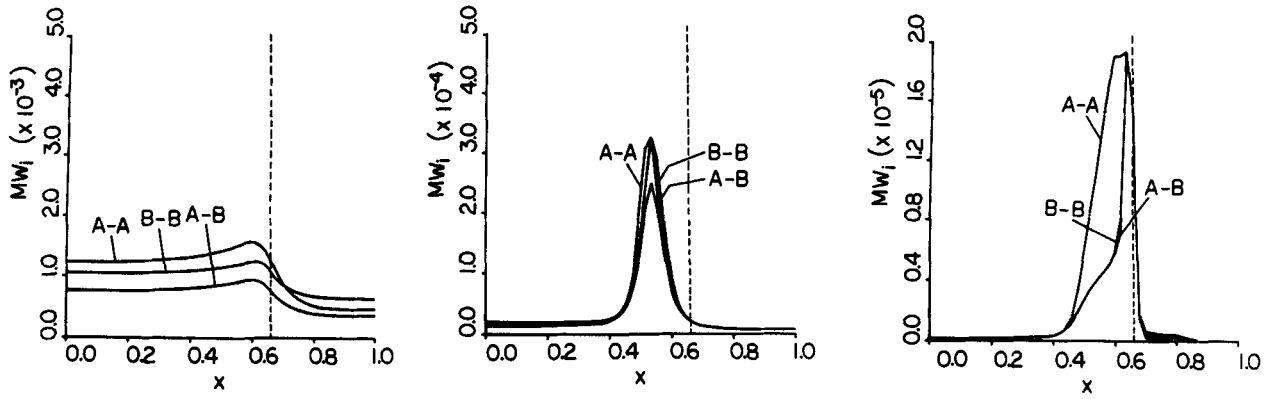

Figure 11. Molecular weight profiles, base case parameters.

a. $\tilde{t}$ = 25 s; b. $\tilde{t}$ = 150 s; c. $\tilde{t}$ = 1,250 s

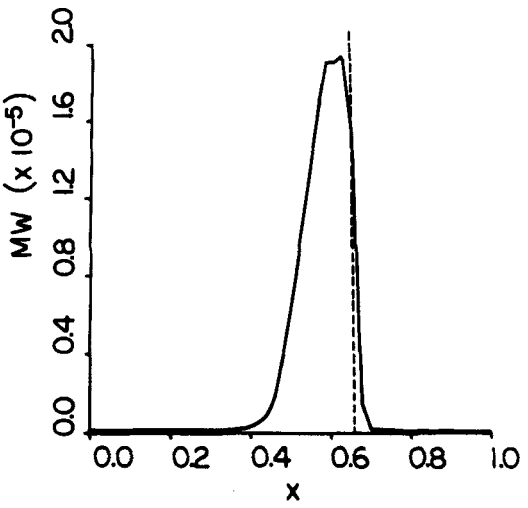

Figure 12. Average molecular weight profile, base case parameters, $\tilde{t}$ = 1,250 s.

region of polymer formation is shifted to the right. The *A–A DP* profiles are significantly different from those for the *A–B* and *B–B* molecules, especially on the diol side of the interface, since *A–A* molecules cannot react with A_2. These profiles are composed of a region on the lefthand side due to early polymer formation, and a region on the righthand side from conversion of *A–B* and *B–B* molecules to *A–A* molecules.

Figures 11a–c give the number-average molecular weight (*MW*) profiles for the three polymer species at short, moderate, and long times, respectively. These profiles exhibit the same behavior as the *DP* profiles. Note that all three species have nearly the same *MW* profiles at short and moderate times since there is much "communication" between species types in a step growth polymerization. The long-time average *MW* profile is displayed in Figure 12, and it has a maximum on the diol side of the interface since the catalyst is initially present on that side of the interface.

Figure 13a shows the average molecular weight of the system as a function of time. Note that the *MW* builds rapidly after an induction period and that nearly all the monomer is incorporated into the polymer chains by the end of this period. The *MW* levels off because the polymer is not mobile in this model, and reactive ends become trapped. This may be seen by comparing time sequences of the zero moment profiles shown in Figure 8 to Figure 13a. The maximum molecular weight across the striation

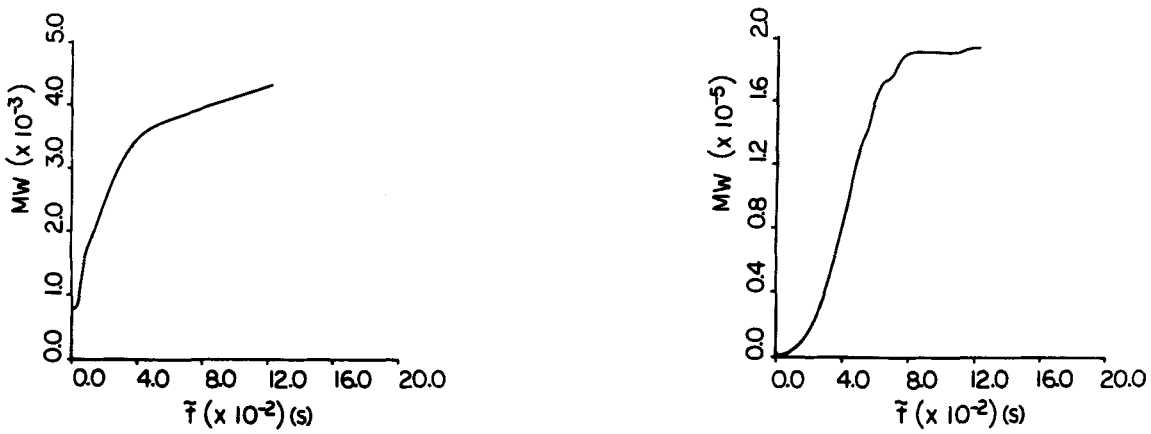

Figure 13. Molecular weight vs. time, base case parameters.

a. Average; b. maximum

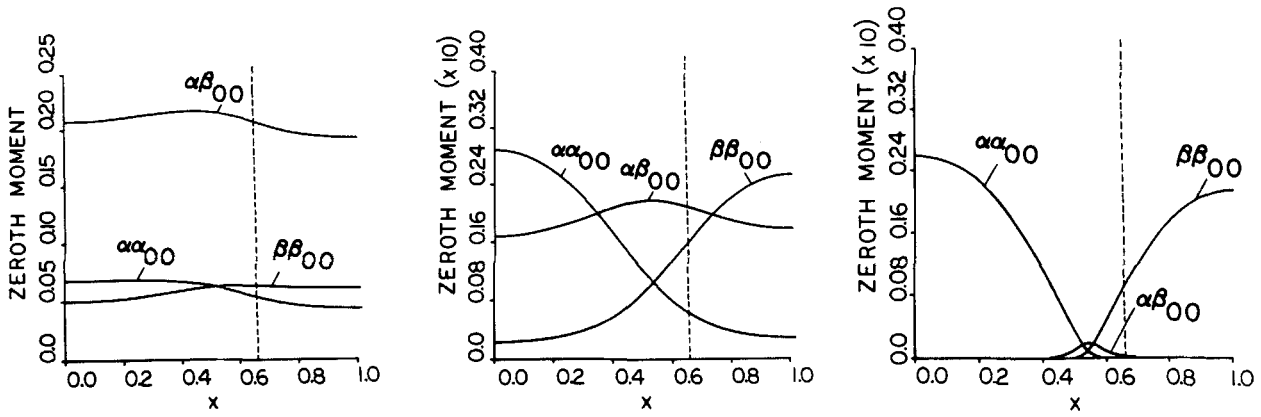

Figure 14. Zero moment profiles, striation thickness decreased by 5×.

a. $\tilde{t}$ = 25 s; b. $\tilde{t}$ = 50 s; c. $\tilde{t}$ = 250 s

is presented vs. time in Figure 13b. It builds rapidly and then levels off, as the average molecular weight did. The fluctuations in Figure 13b are due to the nodal nature of the simulation. The maximum molecular weight across the striation is often more than an order of magnitude higher than the average molecular weight. This may be observed in Figures 11b and 11c.

Mixing level effects

This model is very mixing-sensitive, even more so than the lumped model. Runs were made varying the striation thickness while holding all other parameters constant. The range of mixing levels explored includes striation thicknesses five times smaller than the base case (base case $\tilde{s}$ = 0.01 cm) to five times larger than the base case. This corresponds to a Damköhler number range of 6.0×10^{-1} to 3.8×10^{2}. In addition, the simulation was also run for perfectly mixed conditions (flat spatial profiles).

Zero moment profiles

The zero moment profiles show significant micromixing effects. This is evident upon considering the time sequence shown in Figure 8 (base case), Figure 14 (base case $\tilde{s}$ decreased 5×), and Figure 15 (base case $\tilde{s}$ increased 5×). At small striation thicknesses the profiles are flat, with the same qualitative behavior displayed in the base case. At large striation thicknesses, however, all three polymer zero moments form peaks in the neighborhood of the interface. The qualitative positions are similar to those in the base case. Even for long times, Figure 15c, however, nearly no polymer endgroups are located at the centerlines of the striations. Incomplete monomer conversion occurs under these conditions due to the impervious polymer layer formed near the original interface.

Molecular weight profiles

The molecular weight profiles also show severe micromixing effects. Figure 12 (base case), Figure 16a (base case $\tilde{s}$ decreased 5×), and Figure 16b (base case $\tilde{s}$ increased 5×) indicate that the spatial heterogeneity of the *MW* is decreased with better mixing, and the average *MW* of the system is increased with better mixing (note scales).

Average and maximum molecular weight vs. time

The average molecular weight is plotted vs. time for several striation thicknesses in Figure 17. The well-mixed case is included for comparison. As the striation thickness is increased (poorer mixing), the initial rate of *MW* build is decreased and the asymptote in the molecular weight curve decreases, due to reactant endgroup trapping. The final molecular weight

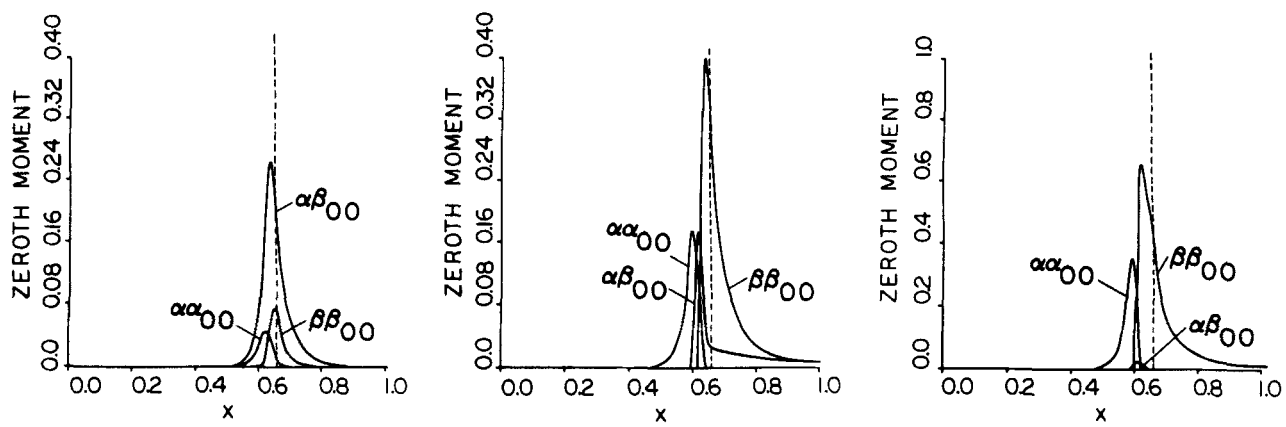

Figure 15. Zero moment profiles, striation thickness increased by 5×.

a. $\tilde{t}$ = 50 s; b. $\tilde{t}$ = 250 s; c. $\tilde{t}$ = 2,250 s

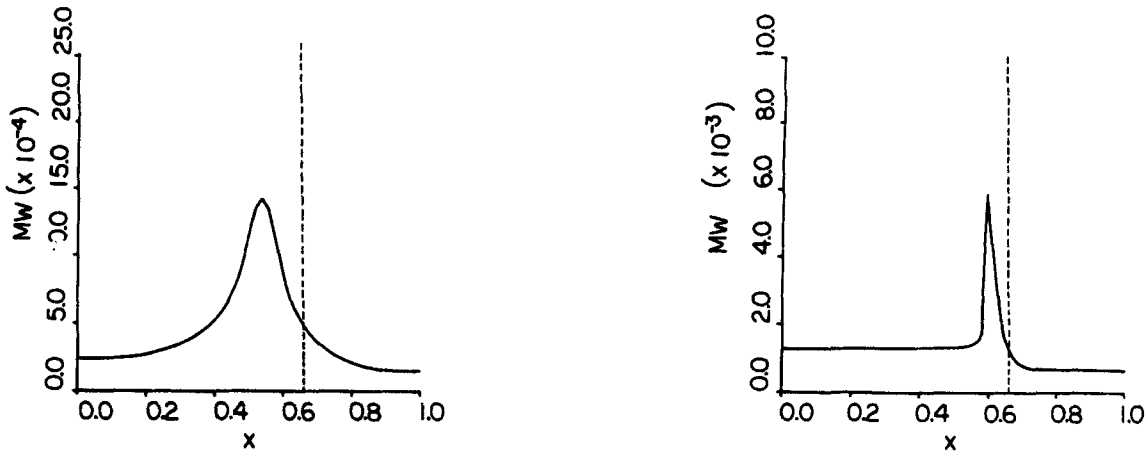

Figure 16. Average molecular weight profile.

a. Striation thickness decreased 5×, $\tilde{t}$ = 250 s

b. Striation thickness increased 5×, $\tilde{t}$ = 2,250 s

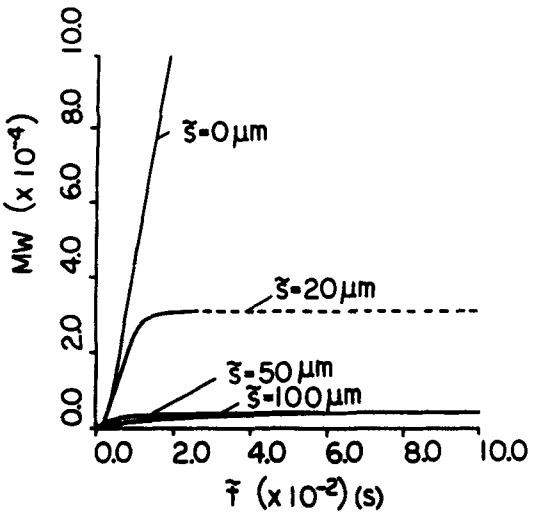

Figure 17. Average molecular weight vs. time as a function of striation thickness.

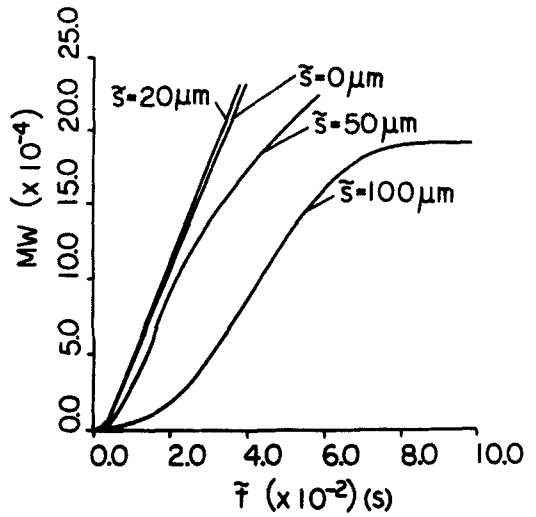

Figure 18. Maximum molecular weight vs. time as a function of striation thickness.

achieved in an unpremixed polymerization is severely affected by the level of reactant segregation. In contrast, the well-mixed case shows a MW that increases without bound. This is expected, however, because at $\tilde{t} = \infty$ there is one chain of infinite molecular weight for a stoichiometric step growth polymerization.

The maximum molecular weight across the striation is shown for several striation thicknesses in Figure 18. Again, as the level of micromixing is decreased, the initial rate of MW growth and the final asymptote are decreased. An interesting anomaly appears. For unpremixed cases approaching the well-mixed case, imperfect mixing yields a higher maximum molecular weight than the well-mixed molecular weight gives (at the same time). This is due to the overlap of higher monomer concentrations in the neighborhood of the interface when compared to the lower, but uniform, monomer concentrations in the well-mixed case.

Comparison at the practical extent of reaction

In order to make a rational comparison of experimental data and modeling simulations, Chella and Ottino (1983) defined a quantity called the asymptotic conversion, or the practical extent of reaction, which is the conversion attained when the rate at which the system is changing falls below some specified small value. Here we take a cutoff for RIM systems as the point at which the rate of adiabatic temperature rise drops below 1°C/min. The corresponding time, denoted $\tilde{t}_\infty$, is plotted vs. striation thickness in Figure 19a. As the striation thickness is increased, $\tilde{t}_\infty$ increases and then decreases. This is because, for moderate values of $\tilde{s}$, it takes longer to reach essentially complete conversion of the reactants for larger striation thicknesses. But, at large values of $\tilde{s}$, the rate at which the temperature rises early in the polymerization is limited by diffusional resistances, resulting in effective shutdown of the reaction at short times.

Figure 19b shows the fraction of long diol remaining unreacted at $\tilde{t}_\infty$ as a function of striation thickness. This shows that a significant fraction of the long diol may be left unreacted at the practical extent of reaction. At a striation thickness greater than 0.015 cm, most of the long diol is unreacted.

The average and maximum molecular weights plotted at $\tilde{t}_\infty$ vs. striation thickness are given in Figure 19c. The average MW

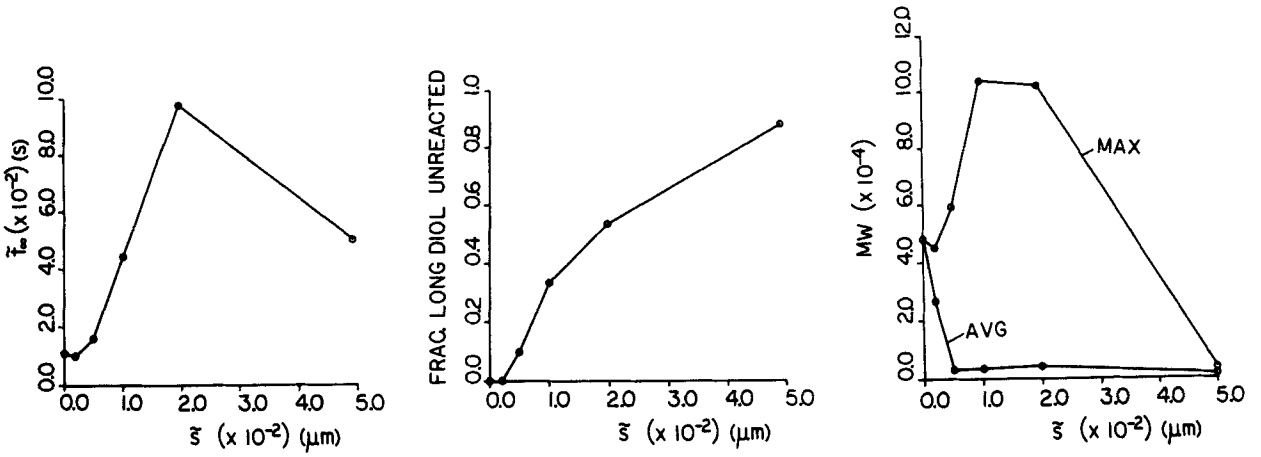

Figure 19.

a. Time for practical extent of reaction vs. striation thickness

b. Fraction of long diol unreacted at $\tilde{t}_\infty$ vs. striation thickness

c. Average and maximum molecular weight at $\tilde{t}_\infty$ vs. striation thickness

decays monotonically with increasing striation thickness, but the maximum MW in the system displays a maximum. This implies that an intermediate mixedness is optimal for building the highest maximum MW in the system if one quenches the polymerization at $\tilde{t}_\infty$.

Conclusions

In summary, the main conclusions are:

1. Polymer product segregation results under imperfectly mixed conditions for a random block copolymerization if the mobilities of the comonomers are significantly different.

2. Under highly segregated conditions (high Damköhler number) the soft segment concentration profile can exhibit two peaks due to reactive endgroup trapping.

3. Both models predict that under poorly mixed conditions, phase separation (soft/hard/soft/hard layering) may occur due to diffusion-reaction interactions; see also (2) above.

4. Under segregated conditions, diol and diisocyanate endgroups become trapped on opposite sides of the interface. This leads to an asymptote in the molecular weight-time behavior.

5. Reactant segregation produces a heterogeneous spatial molecular weight profile, with variations of more than one order of magnitude possible.

6. At the practical extent of reaction the maximum molecular weight across the striation for segregated systems is often larger than the average molecular weight for well-mixed conditions.

7. A large fraction of the long diol (>50%) may remain unreacted for long times, even when the overall stoichiometry is satisfied, for highly segregated conditions.

8. The average molecular weight of the system decreases dramatically as segregation increases.

Acknowledgment

The authors gratefully acknowledge the financial support of CU-MIRP, the Center for University of Massachusetts-Industry Research on Polymers, the donors of the Petroleum Research Fund, administered by the American Chemical Society, and the National Science Foundation through Grant CBT-8513686.

Notation

A^e = triol endgroup
A_1 = short diol (chain extender)
A_2 = long diol
A_1^e = short diol endgroup
A_2^e = long diol endgroup
$AA_{n,m}$ = $A \ldots A$ molecule containing n A_1 and m A_2 molecules
$AB_{n,m}$ = $A \ldots B$ molecule containing n A_1 and m A_2 molecules
$AA(s_1, s_2)$ = generating function for AA molecules
$AB(s_1, s_2)$ = generating function for AB molecules
B = diisocyanate
B^e = diisocyanate endgroup
$BB_{n,m}$ = $B \ldots B$ molecule containing n A_1 and m A_2 molecules
$BB(s_1, s_2)$ = generating function for BB molecules
C = catalyst
$\tilde{C}_i$ = dimensional concentration of species i
$\tilde{C}_i^0$ = initial concentration of species i
$C_i = \tilde{C}_i/\tilde{C}_i^0$ = dimensionless concentration of species i
$\tilde{C}_I^0$ = reference concentration
$\tilde{C}_i^e$ = concentration of endgroups of species i
$\tilde{C}_i^{e0}$ = initial concentration of endgroups of species i
$C_i^e = \tilde{C}_i^e/\tilde{C}_i^{e0}$ = dimensionless concentration of endgroups of species i
C_p = heat capacity
c^* = catalyst exponent for all polymerization rate expressions
$\tilde{D}_i$ = diffusion coefficient of species i
$\tilde{D}_i^0$ = reference diffusion coefficient of species i
$D_i = \tilde{D}_i/\tilde{D}_i^0$ = dimensionless diffusion coefficient of species i
$\tilde{D}_I^0$ = reference diffusion coefficient
$\tilde{D}_i^e$ = diffusion coefficient of endgroups of species i
$\tilde{D}_i^{e0}$ = reference diffusion coefficient of endgroups of species i
$D_i^e = \tilde{D}_i^e/\tilde{D}_i^{e0}$ = dimensionless diffusion coefficient of endgroups of species i
D_i^T = dimensionless temperature component of D_i
D_i^C = dimensionless concentration component of D_i
$D_{am} = \tilde{t}_D/\tilde{t}_R = (|\tilde{r}_I^0|\tilde{s}^2)/(\tilde{D}_I^0\tilde{C}_I^0)$ = second Damköhler number
$DP_{XX(A_1)}$ = degree of polymerization of A_1 monomer in polymer type XX where XX is AA, AB, or BB
$DP_{XX(A_2)}$ = degree of polymerization of A_2 monomer in polymer type XX where XX is AA, AB, or BB
E = activation energy for all polymerization reactions
E_i^d = activation energy for diffusion of species i
E_1 = activation energy for hard segment reaction
E_2 = activation energy for soft segment reaction
ΔH_R = heat of reaction per mole of diisocyanate groups
k_1 = rate constant for hard segment reaction
k_2 = rate constant for soft segment reaction
$k = k'' \exp(-E/R\tilde{T})$

k'' = rate constant for all polymerization reactions
MW_i = molecular weight of species i
MW_{XX} = molecular weight of polymer type XX where XX is AA, AB, or BB
MW = average molecular weight
P = polymer segment
P_1 = hard segment
P_2 = soft segment
$\tilde{r}_i$ = rate of production of species i
$r_i = \tilde{r}_i/|\tilde{r}_I^0|$ = dimensionless rate of production of species i (I is a reference species)
$\tilde{r}_i^e$ = rate of production of endgroups species i
$r_i^e = \tilde{r}_i^e/|\tilde{r}_I^e|$ = dimensionless rate of production of endgroups of species i (I is a reference species)
$r_i^{\square} = D_{am}\xi_i r_i$
R = gas constant
$\tilde{s}$ = striation thickness
$\tilde{s}_A$ = ½ striation thickness of diol phase
$\tilde{s}_B$ = ½ striation thickness of diisocyanate phase
$s_A = \tilde{s}_A/\tilde{s}$ = fraction of striation occupied by diol phase
$s_B = \tilde{s}_B/\tilde{s}$ = fraction of striation occupied by diisocyanate phase
s_1 = dummy variable in generating function formulation
s_2 = dummy variable in generating function formulation
$\tilde{t}$ = time
$\tilde{t}_D$ = characteristic time for diffusion
$t = \tilde{t}/\tilde{t}_D$ = dimensionless time
$\tilde{t}_\infty$ = time for practical extent of reaction
$\tilde{T}$ = temperature
$\tilde{T}^0$ = initial temperature
$T = \tilde{T}/\tilde{T}^0$ = dimensionless temperature
$\tilde{V}_i$ = volume of species i
$\tilde{x}$ = distance
$x = \tilde{x}/\tilde{s}$ = dimensionless distance
$\overline{}$ = spatial average

Greek letters

$\tilde{\alpha}\tilde{\alpha}_{kl}$ = MWD moments for AA molecules
$\tilde{\alpha}\tilde{\beta}_{kl}$ = MWD moments for AB molecules
$\tilde{\beta}\tilde{\beta}_{kl}$ = MWD moments for BB molecules
$\alpha\alpha_{kl}$ = dimensionless MWD moments for AA molecules, Table A2
$\alpha\beta_{kl}$ = dimensionless MWD moments for AB molecules, Table A2
$\beta\beta_{kl}$ = dimensionless MWD moments for BB molecules, Table A2
$\beta_1 - \beta_6$ = dimensionless coefficients, Table A2
γ = dimensionless coefficient in energy balance
$\Delta_i = \tilde{D}_i^0/\tilde{D}_I^0$ = initial diffusivity ratio
$\xi_i = \tilde{C}_I^0/\tilde{C}_i^0$ = initial concentration ratio
$\tilde{\mu}_i$ = viscosity of species i
$\tilde{\mu}_B$ = reference viscosity (chosen to be the viscosity of B)
ϕ_i = volume fraction of species i
ρ_i = density of species i

Appendix: Derivation of Moment Equations from Kinetic Source Terms

Since the polymer species $AA_{n,m}$, $AB_{n,m}$, and $BB_{n,m}$ contain two types of A monomers, we must use double moments to keep track of the state of the system. We may define the moments for $AB_{n,m}$ molecules as:

$$\tilde{\alpha}\tilde{\beta}_{kl} = \sum_{n=0}^{\infty}\sum_{m=0}^{\infty} n^k m^l \tilde{C}_{AB_{n,m}} \tag{A1}$$

Thus, the zero and first moments are:

$$\tilde{\alpha}\tilde{\beta}_{00} = \sum_{n=0}^{\infty}\sum_{m=0}^{\infty} \tilde{C}_{AB_{n,m}} \tag{A2}$$

$$\tilde{\alpha}\tilde{\beta}_{10} = \sum_{n=0}^{\infty}\sum_{m=0}^{\infty} n\tilde{C}_{AB_{n,m}} \tag{A3}$$

$$\tilde{\alpha}\tilde{\beta}_{01} = \sum_{n=0}^{\infty}\sum_{m=0}^{\infty} m\tilde{C}_{AB_{n,m}} \tag{A4}$$

The moments for $AA_{n,m}$ and $BB_{n,m}$ are defined in an analogous manner. The zero and first moments have the following physical meanings:

$\tilde{\alpha}\tilde{\beta}_{00}$ = concentration of A---B molecules
$\tilde{\alpha}\tilde{\beta}_{10}$ = concentration of A_1 monomer in A---B molecules
$\tilde{\alpha}\tilde{\beta}_{01}$ = concentration of A_2 monomer in A---B molecules

The moment definitions may be substituted directly into the monomer kinetic source terms, Table 2, to yield:

$$\frac{d\tilde{C}_{A_1}}{d\tilde{t}} = -2k\tilde{C}_{A_1}\tilde{C}_B\tilde{C}_C^{c^*} - k\tilde{C}_{A_1}\tilde{\alpha}\tilde{\beta}_{00}\tilde{C}_C^{c^*} - 2k\tilde{C}_{A_1}\tilde{\beta}\tilde{\beta}_{00}\tilde{C}_C^{c^*} \tag{A5}$$

$$\frac{d\tilde{C}_{A_2}}{d\tilde{t}} = -2k\tilde{C}_{A_2}\tilde{C}_B\tilde{C}_C^{c^*} - k\tilde{C}_{A_2}\tilde{\alpha}\tilde{\beta}_{00}\tilde{C}_C^{c^*} - 2k\tilde{C}_{A_2}\tilde{\beta}\tilde{\beta}_{00}\tilde{C}_C^{c^*} \tag{A6}$$

$$\frac{d\tilde{C}_B}{d\tilde{t}} = -2k\tilde{C}_{A_1}\tilde{C}_B\tilde{C}_C^{c^*} - 2k\tilde{C}_{A_2}\tilde{C}_B\tilde{C}_C^{c^*} - 2k\tilde{C}_B\tilde{\alpha}\tilde{\alpha}_{00}\tilde{C}_C^{c^*} - k\tilde{C}_B\tilde{\alpha}\tilde{\beta}_{00}\tilde{C}_C^{c^*} \tag{A7}$$

There are several convenient methods to use to obtain the molecular weight distribution of the polymer species from the batch reactor mass balances. Ray (1972) describes several methods, including numerical integration, generating functions, Z-transforms, continuous variable approximation, and statistical methods. If one is satisfied with obtaining only the first several moments of the MWD, rather than the complete MWD, generating functions are convenient to use. Howe (1955) used generating functions for a free radical polymerization. Scanlan (1956) used generating functions to solve several random reactions of polymers, including scission and crosslinking. Tirrell et al. (1987) describe these methods in detail.

The generating function method has been used in this work to obtain the moment equations. We may define the following generating functions, with one for each polymer type:

$$AA(s_1, s_2) = \sum_{n=0}^{\infty}\sum_{m=0}^{\infty} s_1^n s_2^m \tilde{C}_{AA_{n,m}} \tag{A8}$$

$$AB(s_1, s_2) = \sum_{n=0}^{\infty}\sum_{m=0}^{\infty} s_1^n s_2^m \tilde{C}_{AB_{n,m}} \tag{A9}$$

$$BB(s_1, s_2) = \sum_{n=0}^{\infty}\sum_{m=0}^{\infty} s_1^n s_2^m \tilde{C}_{BB_{n,m}} \tag{A10}$$

It is then possible to transform each polymer species batch reactor mass balance into the generating function domain by multiplying each side of the equation by $s_1^n s_2^m$ and summing each side over n and m from zero to infinity. First, transforming the mass

balance for $AA_{n,m}$:

$$\frac{dAA(s_1, s_2)}{d\tilde{t}} = -2k\tilde{C}_B AA(s_1, s_2)\tilde{C}_C^{c*} - kAA(s_1, s_2)AB(s_1 = 1, s_2 = 1)\tilde{C}_C^{c*} + k\sum_{n=0}^{\infty}\sum_{m=0}^{\infty} \cdot \left(s_1^n s_2^m \sum_{i=0}^{n-1}\sum_{j=0}^{m-1} \tilde{C}_{AA_{n-i,m-j}}\tilde{C}_{AB_{i,j}}\right)\tilde{C}_C^{c*} - 2kAA(s_1, s_2)BB(s = 1, s_2 = 1)\tilde{C}_C^{c*} + k\tilde{C}_{A_1}\sum_{n=0}^{\infty}\sum_{m=0}^{\infty} s_1^n s_2^m \tilde{C}_{AB_{n-1,m}}\tilde{C}_C^{c*} + k\tilde{C}_{A_2}\sum_{n=0}^{\infty}\sum_{m=0}^{\infty} s_1^n s_2^m \tilde{C}_{AB_{n,m-1}}\tilde{C}_C^{c*} \quad \text{(A11)}$$

There are three terms in this equation that do not directly reduce to generating function definitions. One needs two shifting relations and one convolution relation to solve this:

$$\sum_{n=0}^{\infty}\sum_{m=0}^{\infty} s_1^n s_2^m \tilde{C}_{AB_{n-1,m}} = s_1 AB(s_1, s_2) \quad \text{(A12)}$$

$$\sum_{n=0}^{\infty}\sum_{m=0}^{\infty} s_1^n s_2^m \tilde{C}_{AB_{n,m-1}} = s_2 AB(s_1, s_2) \quad \text{(A13)}$$

$$\sum_{n=0}^{\infty}\sum_{m=0}^{\infty}\left(s_1^n s_2^m \sum_{i=0}^{n-1}\sum_{j=0}^{m-1} \tilde{C}_{AA_{n-i,m-j}}\tilde{C}_{AB_{i,j}}\right) = AA(s_1, s_2)AB(s_1, s_2) \quad \text{(A14)}$$

These may be substituted into Eq. A11 to yield:

$$\frac{dAA(s_1, s_2)}{d\tilde{t}} = -2k\tilde{C}_B AA(s_1, s_2)\tilde{C}_C^{c*} - kAA(s_1, s_2)AB(s_1 = 1, s_2 = 1)\tilde{C}_C^{c*} + kAA(s_1, s_2)AB(s_1, s_2)\tilde{C}_C^{c*} - 2kAA(s_1, s_2)BB(s_1 = 1, s_2 = 1)\tilde{C}_C^{c*} + k\tilde{C}_{A_1}s_1 AB(s_1, s_2)\tilde{C}_C^{c*} + k\tilde{C}_{A_2}s_2 AB(s_1, s_2)\tilde{C}_C^{c*} \quad \text{(A15)}$$

The mass balances for $AB_{n,m}$ and $BB_{n,m}$ may be transformed in the same manner, using Eqs. A12, A13, and A14, to yield:

$$\frac{dAB(s_1, s_2)}{d\tilde{t}} = 2kAA(s_1, s_2)\tilde{C}_B\tilde{C}_c^{c*} - kAB(s_1, s_2)AA(s_1 = 1, s_2 = 1)\tilde{C}_C^{c*} + 2kAA(s_1, s_2)BB(s_1, s_2)\tilde{C}_C^{c*} - k\tilde{C}_{A_1}AB(s_1, s_2)\tilde{C}_C^{c*} - k\tilde{C}_{A_2}AB(s_1, s_2)\tilde{C}_C^{c*} - k\tilde{C}_B AB(s_1, s_2)\tilde{C}_C^{c*} - kAB(s_1, s_2)AB(s_1 = 1, s_2 = 1)\tilde{C}_C^{c*} + \tfrac{1}{2}kAB(s_1, s_2)AB(s_1, s_2)\tilde{C}_C^{c*} - kAB(s_1, s_2)BB(s_1 = 1, s_2 = 1)\tilde{C}_C^{c*} + 2ks_1\tilde{C}_{A_1}BB(s_1, s_2)\tilde{C}_C^{c*} + 2ks_2\tilde{C}_{A_2}BB(s_1, s_2)\tilde{C}_C^{c*} + 2ks_1\tilde{C}_{A_1}\tilde{C}_B\tilde{C}_C^{c*} + 2ks_2\tilde{C}_{A_2}\tilde{C}_B\tilde{C}_C^{c*} \quad \text{(A16)}$$

$$\frac{dBB(s_1, s_2)}{d\tilde{t}} = -2kBB(s_1, s_2)AA(s_1 = 1, s_2 = 1)\tilde{C}_C^{c*} + k\tilde{C}_B AB(s_1, s_2)\tilde{C}_C^{c*} - kBB(s_1, s_2)AA(s_1 = 1, s_2 = 1)\tilde{C}_C^{c*} + kBB(s_1, s_2)AB(s_1, s_2)\tilde{C}_C^{c*} - 2k\tilde{C}_{A_1}BB(s_1, s_2)\tilde{C}_C^{c*} - 2k\tilde{C}_{A_2}BB(s_1, s_2)\tilde{C}_C^{c*} \quad \text{(A17)}$$

The moments are related simply to the generating functions by:

$$\tilde{\alpha}\tilde{\beta}_{ij} = \lim_{\substack{s_1\to 1\\ s_2\to 1}}\left\{\frac{\partial^i}{\partial(\ln s_1)^i}\frac{\partial^j}{\partial(\ln s_2)^j}[AB(s_1, s_2)]\right\} \quad \text{(A18)}$$

Table A1. Polymer Kinetic Source Term Moment Equations

$$\frac{d\tilde{\alpha}\tilde{\alpha}_{00}}{d\tilde{t}} = -2k\tilde{C}_B\tilde{\alpha}\tilde{\alpha}_{00}\tilde{C}_C^{c*} - 2k\tilde{\alpha}\tilde{\alpha}_{00}\tilde{\beta}\tilde{\beta}_{00}\tilde{C}_C^{c*} + k\tilde{C}_{A_1}\tilde{\alpha}\tilde{\beta}_{00}\tilde{C}_C^{c*} + k\tilde{C}_{A_2}\tilde{\alpha}\tilde{\beta}_{00}\tilde{C}_C^{c*}$$

$$\frac{d\tilde{\alpha}\tilde{\alpha}_{10}}{d\tilde{t}} = -2k\tilde{C}_B\tilde{\alpha}\tilde{\alpha}_{10}\tilde{C}_C^{c*} + k\tilde{\alpha}\tilde{\alpha}_{00}\tilde{\alpha}\tilde{\beta}_{10}\tilde{C}_C^{c*} - 2k\tilde{\alpha}\tilde{\alpha}_{10}\tilde{\beta}\tilde{\beta}_{00}\tilde{C}_C^{c*} + k\tilde{C}_{A_1}\tilde{\alpha}\tilde{\beta}_{00}\tilde{C}_C^{c*} + k\tilde{C}_{A_1}\tilde{\alpha}\tilde{\beta}_{10}\tilde{C}_C^{c*} + k\tilde{C}_{A_2}\tilde{\alpha}\tilde{\beta}_{10}\tilde{C}_C^{c*}$$

$$\frac{d\tilde{\alpha}\tilde{\alpha}_{01}}{d\tilde{t}} = -2k\tilde{C}_B\tilde{\alpha}\tilde{\alpha}_{01}\tilde{C}_C^{c*} + k\tilde{\alpha}\tilde{\alpha}_{00}\tilde{\alpha}\tilde{\beta}_{01}\tilde{C}_C^{c*} - 2k\tilde{\alpha}\tilde{\alpha}_{01}\tilde{\beta}\tilde{\beta}_{00}\tilde{C}_C^{c*} + k\tilde{C}_{A_1}\tilde{\alpha}\tilde{\beta}_{01}\tilde{C}_C^{c*} + k\tilde{C}_{A_2}\tilde{\alpha}\tilde{\beta}_{01}\tilde{C}_C^{c*} + k\tilde{C}_{A_2}\tilde{\alpha}\tilde{\beta}_{00}\tilde{C}_C^{c*}$$

$$\frac{d\tilde{\alpha}\tilde{\beta}_{00}}{d\tilde{t}} = 2k\tilde{\alpha}\tilde{\alpha}_{00}\tilde{C}_B\tilde{C}_C^{c*} - k\tilde{\alpha}\tilde{\beta}_{00}\tilde{\alpha}\tilde{\alpha}_{00}\tilde{C}_C^{c*} + 2k\tilde{\alpha}\tilde{\alpha}_{00}\tilde{\beta}\tilde{\beta}_{00}\tilde{C}_C^{c*} - k\tilde{C}_{A_1}\tilde{\alpha}\tilde{\beta}_{00}\tilde{C}_C^{c*} - k\tilde{C}_{A_2}\tilde{\alpha}\tilde{\beta}_{00}\tilde{C}_C^{c*} - k\tilde{C}_B\tilde{\alpha}\tilde{\beta}_{00}\tilde{C}_C^{c*} - \tfrac{1}{2}k\tilde{\alpha}\tilde{\beta}_{00}\tilde{\alpha}\tilde{\beta}_{00}\tilde{C}_C^{c*} - k\tilde{\alpha}\tilde{\beta}_{00}\tilde{\beta}\tilde{\beta}_{00}\tilde{C}_C^{c*} + 2k\tilde{C}_{A_1}\tilde{\beta}\tilde{\beta}_{00}\tilde{C}_C^{c*} + 2k\tilde{C}_{A_2}\tilde{\beta}\tilde{\beta}_{00}\tilde{C}_C^{c*} + 2k\tilde{C}_{A_1}\tilde{C}_B\tilde{C}_C^{c*} + 2k\tilde{C}_{A_2}\tilde{C}_B\tilde{C}_C^{c*}$$

$$\frac{d\tilde{\alpha}\tilde{\beta}_{10}}{d\tilde{t}} = 2k\tilde{\alpha}\tilde{\alpha}_{10}\tilde{C}_B\tilde{C}_C^{c*} - k\tilde{\alpha}\tilde{\beta}_{10}\tilde{\alpha}\tilde{\alpha}_{00}\tilde{C}_C^{c*} + 2k\tilde{\alpha}\tilde{\alpha}_{10}\tilde{\beta}\tilde{\beta}_{00}\tilde{C}_C^{c*} + 2k\tilde{\alpha}\tilde{\alpha}_{00}\tilde{\beta}\tilde{\beta}_{10}\tilde{C}_C^{c*} - k\tilde{C}_{A_1}\tilde{\alpha}\tilde{\beta}_{10}\tilde{C}_C^{c*} - k\tilde{C}_{A_2}\tilde{\alpha}\tilde{\beta}_{10}\tilde{C}_C^{c*} - k\tilde{C}_B\tilde{\alpha}\tilde{\beta}_{10}\tilde{C}_C^{c*} - k\tilde{\alpha}\tilde{\beta}_{10}\tilde{\beta}\tilde{\beta}_{00}\tilde{C}_C^{c*} + 2k\tilde{C}_{A_1}\tilde{\beta}\tilde{\beta}_{10}\tilde{C}_C^{c*} + 2k\tilde{C}_{A_1}\tilde{\beta}\tilde{\beta}_{00}\tilde{C}_C^{c*} + 2k\tilde{C}_{A_2}\tilde{\beta}\tilde{\beta}_{10}\tilde{C}_C^{c*} + 2k\tilde{C}_{A_1}\tilde{C}_B\tilde{C}_C^{c*}$$

$$\frac{d\tilde{\alpha}\tilde{\beta}_{01}}{d\tilde{t}} = 2k\tilde{\alpha}\tilde{\alpha}_{01}\tilde{C}_B\tilde{C}_C^{c*} - k\tilde{\alpha}\tilde{\beta}_{01}\tilde{\alpha}\tilde{\alpha}_{00}\tilde{C}_C^{c*} + 2k\tilde{\alpha}\tilde{\alpha}_{01}\tilde{\beta}\tilde{\beta}_{00}\tilde{C}_C^{c*} + 2k\tilde{\alpha}\tilde{\alpha}_{00}\tilde{\beta}\tilde{\beta}_{01}\tilde{C}_C^{c*} - k\tilde{C}_{A_1}\tilde{\alpha}\tilde{\beta}_{01}\tilde{C}_C^{c*} - k\tilde{C}_{A_2}\tilde{\alpha}\tilde{\beta}_{01}\tilde{C}_C^{c*} - k\tilde{C}_B\tilde{\alpha}\tilde{\beta}_{01}\tilde{C}_C^{c*} - k\tilde{\alpha}\tilde{\beta}_{01}\tilde{\beta}\tilde{\beta}_{00}\tilde{C}_C^{c*} + 2k\tilde{C}_{A_1}\tilde{\beta}\tilde{\beta}_{01}\tilde{C}_C^{c*} + 2k\tilde{C}_{A_2}\tilde{\beta}\tilde{\beta}_{00}\tilde{C}_C^{c*} + 2k\tilde{C}_{A_2}\tilde{C}_B\tilde{C}_C^{c*}$$

$$\frac{d\tilde{\beta}\tilde{\beta}_{00}}{d\tilde{t}} = -2k\tilde{\beta}\tilde{\beta}_{00}\tilde{\alpha}\tilde{\alpha}_{00}\tilde{C}_C^{c*} + k\tilde{C}_B\tilde{\alpha}\tilde{\beta}_{00}\tilde{C}_C^{c*} - 2k\tilde{C}_{A_1}\tilde{\beta}\tilde{\beta}_{00}\tilde{C}_C^{c*} - 2k\tilde{C}_{A_2}\tilde{\beta}\tilde{\beta}_{00}\tilde{C}_C^{c*}$$

$$\frac{d\tilde{\beta}\tilde{\beta}_{10}}{d\tilde{t}} = -2k\tilde{\beta}\tilde{\beta}_{10}\tilde{\alpha}\tilde{\alpha}_{00}\tilde{C}_C^{c*} + k\tilde{C}_B\tilde{\alpha}\tilde{\beta}_{10}\tilde{C}_C^{c*} + k\tilde{\beta}\tilde{\beta}_{00}\tilde{\alpha}\tilde{\beta}_{10}\tilde{C}_C^{c*} - 2k\tilde{C}_{A_1}\tilde{\beta}\tilde{\beta}_{10}\tilde{C}_C^{c*} - 2k\tilde{C}_{A_2}\tilde{\beta}\tilde{\beta}_{10}\tilde{C}_C^{c*}$$

$$\frac{d\tilde{\beta}\tilde{\beta}_{01}}{d\tilde{t}} = -2k\tilde{\beta}\tilde{\beta}_{01}\tilde{\alpha}\tilde{\alpha}_{00}\tilde{C}_C^{c*} + k\tilde{C}_B\tilde{\alpha}\tilde{\beta}_{01}\tilde{C}_C^{c*} + k\tilde{\beta}\tilde{\beta}_{00}\tilde{\alpha}\tilde{\beta}_{01}\tilde{C}_C^{c*} - 2k\tilde{C}_{A_1}\tilde{\beta}\tilde{\beta}_{01}\tilde{C}_C^{c*} - 2k\tilde{C}_{A_2}\tilde{\beta}\tilde{\beta}_{01}\tilde{C}_C^{c*}$$

Table A2. Definitions of Dimensionless Variables for Kinetic Source Terms

$$C_{A_1} = \frac{\tilde{C}_{A_1}}{\tilde{C}^0_{A_1}} \qquad C_{A_2} = \frac{\tilde{C}_{A_2}}{\tilde{C}^0_{A_2}} \qquad C_B = \frac{\tilde{C}_B}{\tilde{C}^0_B} \qquad C_C = \frac{\tilde{C}_C}{\tilde{C}^0_C}$$

$$\alpha\alpha_{00} = \frac{\tilde{\alpha}\tilde{\alpha}_{00}}{\tilde{C}^0_{A_1} + \tilde{C}^0_{A_2}} \qquad \alpha\alpha_{10} = \frac{\tilde{\alpha}\tilde{\alpha}_{10}}{\tilde{C}^0_{A_1}} \qquad \alpha\alpha_{01} = \frac{\tilde{\alpha}\tilde{\alpha}_{01}}{\tilde{C}^0_{A_2}}$$

$$\alpha\beta_{00} = \frac{\tilde{\alpha}\tilde{\beta}_{00}}{\tilde{C}^0_{A_1} + \tilde{C}^0_{A_2}} \qquad \alpha\beta_{10} = \frac{\tilde{\alpha}\tilde{\beta}_{10}}{\tilde{C}^0_{A_1}} \qquad \alpha\beta_{01} = \frac{\tilde{\alpha}\tilde{\beta}_{01}}{\tilde{C}^0_{A_2}}$$

$$\beta\beta_{00} = \frac{\tilde{\beta}\tilde{\beta}_{00}}{\tilde{C}^0_{A_1} + \tilde{C}^0_{A_2}} \qquad \beta\beta_{10} = \frac{\tilde{\beta}\tilde{\beta}_{10}}{\tilde{C}^0_{A_1}} \qquad \beta\beta_{01} = \frac{\tilde{\beta}\tilde{\beta}_{01}}{\tilde{C}^0_{A_2}}$$

$$\beta_1 = \frac{k(\bar{s})^2(\tilde{C}^0_B)(\tilde{C}^0_C)^{c*}}{\tilde{D}^0_{A_1}} \qquad \beta_2 = \frac{k(\bar{s})^2(\tilde{C}^0_{A_1} + \tilde{C}^0_{A_2})(\tilde{C}^0_C)^{c*}}{\tilde{D}^0_{A_1}}$$

$$\beta_3 = \frac{k(\bar{s})^2(\tilde{C}^0_{A_1})(\tilde{C}^0_C)^{c*}}{\tilde{D}^0_{A_1}} \qquad \beta_4 = \frac{k(\bar{s})^2(\tilde{C}^0_{A_2})(\tilde{C}^0_C)^{c*}}{\tilde{D}^0_{A_1}}$$

$$\beta_5 = \frac{k(\bar{s})^2(\tilde{C}^0_{A_1})(\tilde{C}^0_B)(\tilde{C}^0_C)^{c*}}{\tilde{D}^0_{A_1}(\tilde{C}^0_{A_1} + \tilde{C}^0_{A_2})} \qquad \beta_6 = \frac{k(\bar{s})^2(\tilde{C}^0_{A_2})(\tilde{C}^0_B)(\tilde{C}^0_C)^{c*}}{\tilde{D}^0_{A_1}(\tilde{C}^0_{A_1} + \tilde{C}^0_{A_2})}$$

$$t = \tilde{t}/[(\bar{s})^2/\tilde{D}^0_{A_1}]$$

Thus, the zero and first moments are given by:

$$\tilde{\alpha}\tilde{\beta}_{00} = \lim_{\substack{s_1 \to 1 \\ s_2 \to 1}} \{[AB(s_1, s_2)]\} \tag{A19}$$

$$\tilde{\alpha}\tilde{\beta}_{10} = \lim_{\substack{s_1 \to 1 \\ s_2 \to 1}} \left\{\frac{\partial}{\partial(\ln s_1)}[AB(s_1, s_2)]\right\} \tag{A20}$$

$$\tilde{\alpha}\tilde{\beta}_{01} = \lim_{\substack{s_1 \to 1 \\ s_2 \to 1}} \left\{\frac{\partial}{\partial(\ln s_2)}[AB(s_1, s_2)]\right\} \tag{A21}$$

Analogous relationships hold for $\tilde{\alpha}\tilde{\alpha}_{ij}$ and $\tilde{\beta}\tilde{\beta}_{ij}$. By doing the operations specified in Eqs. A19, A20, and A21, one obtains the batch reactor moment equations presented in Table A1.

The monomer kinetic source terms, Eqs. A5–A7, and the polymer source term moment equations, Table A1, are used in the simulation. By applying the dimensionless kinetic variable definitions in Table A2 to these equations the dimensionless kinetic source terms may be obtained. These are listed in Table 4 in the text.

Literature cited

Bird, R. B., W. E. Stewart, and E. N. Lightfoot. *Transport Phenomena,* Wiley, New York (1960).

Chang, A. L., R. M. Briber, E. L. Thomas, R. J. Zdrahala, and F. E. Critchfield, "Morphological Study of the Structure Developed During the Polymerization of a Series of Segmented Polyurethanes," *Polymer,* **23,** 1060 (1982).

Chella, R., and J. M. Ottino, "Simplified Model for Mechanical Mixing Diffusion, and Reaction in a Single Screw Extruder," *Am. Chem. Soc. Symp. Ser.,* **196,** 567 (1982).

———, "Modeling of Rapidly Mixed Fast-Crosslinking Exothermic Polymerizations. I: Adiabatic Temperature Rise," *AIChE J.,* **29,** 373 (1983).

———, "Conversion and Selectivity Modifications Due to Mixing in Unpremixed Reactors," *Chem. Eng. Sci.,* **39,** 551 (1984).

Chen, C. H. Y., R. M. Briber, E. L. Thomas, M. Xu, and W. J. MacKnight, "Structure and Morphology of Segmented Polyurethanes. 2: Influence of Reactant Incompatibility," *Polymer,* **24,** 1333 (1983).

Cussler, E. L., *Diffusion-Mass Transfer in Fluid Systems,* Cambridge Press, Cambridge (1984).

Fields, S. D., "Mixing Effects in Unpremixed Polymerizations," Ph.D. Diss., Univ. Massachusetts, Amherst, (1985).

Fields, S. D., and J. M. Ottino, "Effect of Striation Thickness Distribution on the Course of an Unpremixed Polymerization," accepted, *Chem. Eng. Sci.,* (1987a).

———, "Effect of Stretching Path on the Course of Polymerizations: Applications to Idealized Unpremixed Reactors," accepted, *Chem. Eng. Sci.,* (1987b).

Fields, S. D., E. L. Thomas, and J. M. Ottino, "Visualization of Interfacial Urethane Polymerizations by Means of a New Microstage Reactor," *Polymer,* **27,** 1423 (1986).

Hindmarsh, A. C., "GEARB: Solution of Ordinary Differential Equations Having Banded Jacobian" Lawrence-Livermore Lab., CA (1977).

Howe, J. P., "Method of Integrating the Rate Equations for Free-Radical-Initiated Polymerizations," *J. Chem. Phys.,* **23,** 899 (1955).

Kendall, J., and K. P. Monroe, "The Viscosity of Liquids. II: The Viscosity-Composition Curve for Ideal Liquid Mixtures," *J. Am. Chem. Soc.,* **39,** 1787 (1917).

Kolodziej, P., C. W. Macosko, and W. E. Ranz, "The Influence of Impingement Mixing on Striation Thickness Distribution and Properties in Fast Polyurethane Polymerization," *Polym. Eng. Sci.,* **22,** 388 (1982).

Lee, L. J., J. M. Ottino, W. E. Ranz, and C. W. Macosko, "Impingement Mixing in Reaction Injection Molding," *Polym. Eng. Sci.,* **20,** 868 (1980).

Millick, F., and C. E. Carraher, Jr., eds., *Interfacial Synthesis,* V. 1, Dekker, New York (1977).

Ottino, J. M., and R. Chella, "Mixing of Polymeric Liquids: A Brief Review and Recent Theoretical Developments," *Polym. Eng. Sci.,* **23,** 357 (1983).

Ranz, W. E., "Application of a Stretch Model to Mixing, Diffusion, and Reaction in Laminar and Turbulent Flows," *AIChE J.,* **25,** 41 (1979).

Ray, W. H., "On the Mathematical Modeling of Polymerization Reactors," *J. Macromol. Sci.—Revs. Macromol. Chem.,* **C8,** 1 (1972).

Richter, E. B., and C. W. Macosko, "Kinetics of Fast (RIM) Urethane Polymerization," *Polym. Eng. Sci.,* **18,** 1012 (1978).

Scanlan, J., "Molecular Weight Distribution Functions in Random Reaction Polymers," *Trans. Faraday Soc.,* **52,** 1286 (1956).

Tirrell, M., R. Galvan and R. L. Laurence, "Polymerization Reactors," J. J. Carberry and A. Varma, eds., Chem. Reaction and Reactor Engr., Dekker, New York 735 (1987).

Manuscript received Nov. 15, 1985, and revision received Jan. 6, 1987.